ARCHIVES OF MECHANICS **Appears since 1949**

Aims and Scope

ARCHIVES OF MECHANICS provides a forum for original research on mechanics of solids, fluids and discrete systems, including the development of mathematical methods for solving mechanical problems. The journal encompasses all aspects of the field, with the emphasis placed on:

- mechanics of materials: elasticity, plasticity, time-dependent phenomena, phase transformation, damage, fracture; physical and experimental foundations, micromechanics, thermodynamics, instabilities
- methods and problems in continuum mechanics: general theory and novel applications, thermomechanics, structural analysis, porous media, contact problems
- dynamics of material systems
- fluid flows and interactions with solids

Address of the Editorial Office:
Institute of Fundamental Technological Research
Świętokrzyska 21
PL 00-049 Warsaw, Poland

Tel.(48-22) 826 60 22, Fax (48-22) 826 98 15, E-mail: publikac@ippt.gov.pl

Abstracted/indexed in:

Applied Mechanics Reviews, Current Mathematical Publications, Mathematical Reviews, MathSci, Zentralblatt für Mathematik, UnCover, Inspec.

http://am.ippt.gov.pl/

Polish Academy of Sciences
Institute of Fundamental Technological Research

Archives of Mechanics

Archiwum Mechaniki Stosowanej

volume 54 issue 3

DRUKARNIA BRACI GRODZICKICH

SUBSCRIPTIONS

Address of the Editorial Office: Archives of Mechanics
Institute of Fundamental Technological Research, Świętokrzyska 21
PL 00-049 Warsaw, Poland
Tel. 48 (*prefix*) 22 826 60 22, Fax 48 (*prefix*) 22 826 98 15,
e-mail:publikac@ippt.gov.pl

Subscription orders for all journals edited by IFTR may be sent directly to the Editorial Office of the Institute of Fundamental Technological Research

Subscription rates

Annual subscription rate (2002) including postage is US $ 240.
Please transfer the subscription fee to our bank account: Payee: IPPT PAN,
Bank: PKO SA. IV O/Warszawa,
Account number 12401053-40054492-3000-401112-001.

All journals edited by IFTR are available also through:

- Foreign Trade Enterprise ARS POLONA Krakowskie Przedmieście 7, 00-068 Warszawa, Poland fax 48 (*prefix*) 22 826 86 73
- RUCH S.A. ul. Towarowa 28, 00-958 Warszawa, Poland fax 48 (*prefix*) 22 620 17 62
- International Publishing Service Sp. z o.o. ul. Noakowskiego 10 lok. 38 00-664 Warszawa, Poland tel./fax 48 (*prefix*) 22 625 16 53, 625 49 55

Warunki prenumeraty

Redakcja przyjmuje prenumeratę na wszystkie czasopisma wydawane przez IPPT PAN. Bieżące numery można nabyć, a także zaprenumerować roczne wydanie Archiwum Mechaniki Stosowanej bezpośrednio w Dziale Wydawnictw IPPT PAN, Świętokrzyska 21, 00-049 Warszawa, Tel. 48 (*prefix*) 22 826 60 22; Fax 48 (*prefix*) 22 826 98 15.
Cena rocznej prenumeraty z bonifikatą (na rok 2002) dla krajowego odbiorcy wynosi 300 PLN

Również można je nabyć, a także zamówić (przesyłka za zaliczeniem pocztowym) we Wzorcowni Ośrodka Rozpowszechniania Wydawnictw Naukowych PAN,
00-818 Warszawa, ul. Twarda 51/55, tel. 48 (*prefix*) 22 697 88 35.
Wpłaty na prenumeratę przyjmują także jednostki kolportażowe RUCH S.A. Oddział Krajowej Dystrybucji Prasy, 00-958 Warszawa, ul. Towarowa 28. Konto: PBK. S.A. XIII Oddział Warszawa nr 11101053-16551-2700-1-67. Dostawa odbywa się pocztą lotniczą, której koszt w pełni pokrywa zleceniodawca. Tel. 48 (*prefix*) 22 620 10 39, Fax 48 (*prefix*) 22 620 17 62

Arkuszy wydawniczych 10. Arkuszy drukarskich 6.65
Papier offset. kl III 70g. B1.
Oddano do składania w czerwcu 2002 r. Druk ukończono w czerwcu 2002 r.
Skład w systemie TEX: E. Jaczyńska.
Druk i oprawa: Drukarnia Braci Grodzickich, Piaseczno ul. Geodetów 47A.

Arch. Mech., **54**, 3, pp. 185–198, Warszawa 2002

Influence and Green's functions for orthotropic micropolar continua

RAJNEESH KUMAR and SUMAN CHOUDHARY

Mathematics Department, Kurukshetra University,
Kurukshetra 136 119,
Haryana, INDIA.

THE ARTICLE REPORTS on a methodology to synthesize the response of orthotropic micropolar half-space subjected to concentrated and distributed loads. The disturbance due to normal and tangential loads are investigated by employing the eigenvalue approach. The integral transforms have been inverted by using a numerical technique to obtain the normal displacement, normal force stress and tangential couple stress in the physical domain. The results concerning these quantities are given and illustrated graphically.

Key words: Micropolar, orthotropic, eigenvalue, Fourier and Laplace transforms.

1. Introduction

IN MANY ENGINEERING problems, including the response of soils, geological materials and composites, the assumptions of an isotropic behaviour may not reflect some significant features of the continuum response. The formulation and solution of anisotropic problems is much more difficult and cumbersome than its isotropic counterpart. In the last years the elastodynamic response of anisotropic continuum has received the attention of several reseachers. In particular, transversely isotropic and orthotropic materials, which may not be distinguished from each other in plane strain and plane stress cases, have been more regularly studied.

The theory of micropolar elasticity introduced and developed by ERINGEN [1] rised much interest because of its possible utility in investigating the deformation properties of solids for which the classical theory is inadequate. The micropolar theory is belived to be particularly useful in investigating materials consisting of bar-like molecules which exhibit microrotation effects and which can transmit body and surface couples. Recently, CHENG and HE [11,12], ERBAY [14], KUMAR and DESWAL [15,16] have studied different problems in micropolar isotropic medium.

A review of literature on micropolar orthotropic continua shows that IESAN [3,4,5] analyzed the static problems of plane micropolar strain of a homogeneous and orthotropic elastic solid, torsion problem of homogeneous and orthotropic

cylinders in the linear theory of micropolar elasticity and bending of orthotropic micropolar elastic beams by terminal couples. NAKAMURA *et. al.* [8] derived the finite element method for orthotropic micropolar elasticity.

Most of the problems studied so far, in micropolar elasticity involve the use of potential functions. However, the use of the eigenvalue approach has the advantage of finding the solutions of equations in the coupled form directly, in the matrix notations, whereas the potential function approach requires decoupling of equations. Yet, the eigenvalue approach has not been applied in micropolar orthotropic medium. MAHALANABIS and MANNA [10,13] applied the eigenvalue approach to linear micropolar elasticity by arranging basic equations of linear micropolar elasticity in the form of matrix differential equation. Recently, KUMAR *et. al.* [17] applied the eigenvalue approach to micropolar elastic medium due to impulsive force at the origin.

2. Problem formulation

Let us consider a homogeneous and orthotropic micropolar half-space. The rectangular Cartesian co-ordinate system (x, y, z) having origin on the plane $y = 0$, with y axis directed vertically into the medium is introduced. A normal or tangential source is assumed to be acting at the origin of the rectangular Cartesian co-ordinates.

If we restrict our analysis parallel to the xy-plane with displacement vector $\mathbf{u} = (u_1, u_2, 0)$ and microrotation vector $\boldsymbol{\Phi} = (0, 0, \phi_3)$, the basic equations in the dynamic theory of the plane strain of homogeneous and orthotropic micropolar solids, in absence of body forces and body couples given by ERINGEN [2], can be recalled as:

$$t_{ji,j} = \rho \frac{\partial^2 u_i}{\partial t^2}, \tag{2.1}$$

$$m_{i3,i} + \epsilon_{ij3} t_{ij} = \rho j \frac{\partial^2 \phi_3}{\partial t^2}. \tag{2.2}$$

The constitutive relations, given by IESAN [3], can be written as:

$$\begin{aligned} t_{11} &= A_{11}\epsilon_{11} + A_{12}\epsilon_{22}, \quad t_{12} = A_{77}\epsilon_{12} + A_{78}\epsilon_{21}, \\ t_{21} &= A_{78}\epsilon_{12} + A_{88}\epsilon_{21}, \quad t_{22} = A_{12}\epsilon_{11} + A_{22}\epsilon_{22}, \\ m_{13} &= B_{66}\phi_{3,1}, \quad m_{23} = B_{44}\phi_{3,2}, \end{aligned} \tag{2.3}$$

where

$$\epsilon_{ij} = u_{j,i} + \epsilon_{ji3}\phi_3. \tag{2.4}$$

In these relations, we have used the following notations: t_{ij} – components of the force stress tensor, m_{ij} – component of the couple stress tensor, ϵ_{ij} – component of the micropolar strain tensor, u_i – components of displacement vector, ϕ_3 – component of microrotation vector, ϵ_{ijk} – permutation symbol, $A_{11}, A_{12}, A_{22}, A_{77}, A_{78}, A_{88}, B_{44}, B_{66}$ – characteristic constants of the material, ρ – the density and j – the microinertia.

We introduce the dimensionless quantities

$$
\begin{aligned}
&x^* = \frac{\omega}{c_1}x, \qquad y^* = \frac{\omega}{c_1}y, \qquad u_i^* = \frac{\omega}{c_1}u_i, \qquad \phi_3^* = \frac{A_{11}}{K_1}\phi_3, \\
&t_{ij}^* = \frac{t_{ij}}{A_{11}}, \qquad m_{ij}^* = \frac{c_1}{B_{44}\omega}m_{ij}, \qquad t^* = \omega t,
\end{aligned} \tag{2.5}
$$

where $c_1^2 = A_{11}/\rho$ and $\omega^2 = \chi/\rho j$.

We suppose that initially the half-space is at rest in its undeformed state, i.e., we suppose that the following homogeneous intial conditions hold for $t \geqslant 0$:

$$
u_i(x,y,0) = \frac{\partial u_i}{\partial t} = 0, \qquad \phi_3(x,y,0) = \frac{\partial \phi_3}{\partial t} = 0.
$$

Introducing dimensionless quantities as defined in Eq. (2.5) as well as using homogeneous intial conditions in Eqs. (2.1)-(2.4) (dropping the asterisks for convenience) and applying the Laplace transform w.r. to 't' defined by

$$
\{\overline{u}_i(x,y,p), \overline{\phi}_3(x,y,p)\} = \int_0^\infty \{u_i(x,y,t), \phi_3(x,y,t)\}e^{-pt}dt, \quad i = 1,2 \tag{2.6}
$$

and then the Fourier transform w.r. to 'x' defined by

$$
\{\tilde{u}_i(\xi,y,p), \tilde{\phi}_3(\xi,y,p)\} = \int_{-\infty}^\infty \{\overline{u}_i(x,y,p), \overline{\phi}_3(x,y,p)\}e^{\iota\xi x}dx, \quad i = 1,2 \tag{2.7}
$$

on the resulting expressions, we obtain

$$
\tilde{u''}_1 = Q_{11}\tilde{u}_1 + Q_{15}\tilde{u'}_2 + Q_{16}\tilde{\phi'}_3, \tag{2.8}
$$

$$
\tilde{u''}_2 = Q_{22}\tilde{u}_2 + Q_{23}\tilde{\phi}_3 + Q_{24}\tilde{u'}_1, \tag{2.9}
$$

$$
\tilde{\phi''}_3 = Q_{32}\tilde{u}_2 + Q_{33}\tilde{\phi}_3 + Q_{34}\tilde{u'}_1, \tag{2.10}
$$

where primes in Eqs. (2.8)-(2.10) represent the first and second order differentiation w.r. to y, respectively and

$$Q_{11} = \frac{A_{11}(\xi^2+p^2)}{A_{88}}, \qquad Q_{15} = \frac{\iota\xi(A_{12}+A_{78})}{A_{88}}, \qquad Q_{16} = \frac{K_1^2}{A_{11}A_{88}},$$

$$Q_{22} = \frac{(\xi^2 A_{77}+p^2A_{11})}{A_{22}}, \quad Q_{23} = -\frac{\iota\xi K_1K_2}{A_{11}A_{22}}, \quad Q_{24} = \frac{\iota\xi(A_{12}+A_{78})}{A_{22}},$$

$$Q_{32} = \frac{\iota\xi K_2A_{11}^2}{\omega^2\rho B_{44}K_1},$$

$$Q_{33} = \frac{(\xi^2B_{66}\omega^2+c_1^2\chi)+jp^2\omega^2A_{11}}{B_{44}}, \tag{2.11}$$

$$Q_{34} = -\frac{A_{11}^2}{\rho\omega^2B_{44}},$$

$$K_1 = A_{78}-A_{88}, \quad K_2 = A_{77}-A_{78}, \quad \chi = K_2-K_1.$$

The system of Eqs. (2.8)-(2.10) can be written as

$$\frac{d}{dy}W(\xi,y,p) = A(\xi,p)W(\xi,y,p), \tag{2.12}$$

where

$$W = \begin{bmatrix} U \\ U' \end{bmatrix}, \quad A = \begin{bmatrix} O & I \\ A_2 & A_1 \end{bmatrix}, \quad U = \begin{bmatrix} \tilde{u}_1 \\ \tilde{u}_2 \\ \tilde{\phi}_3 \end{bmatrix},$$

$$O = \begin{bmatrix} 0 & 0 & 0 \\ 0 & 0 & 0 \\ 0 & 0 & 0 \end{bmatrix}, \quad I = \begin{bmatrix} 1 & 0 & 0 \\ 0 & 1 & 0 \\ 0 & 0 & 1 \end{bmatrix}, \tag{2.13}$$

$$A_1 = \begin{bmatrix} 0 & Q_{15} & Q_{16} \\ Q_{24} & 0 & 0 \\ Q_{34} & 0 & 0 \end{bmatrix}, \quad A_2 = \begin{bmatrix} Q_{11} & 0 & 0 \\ 0 & Q_{22} & Q_{23} \\ 0 & Q_{32} & Q_{33} \end{bmatrix}.$$

To solve Eq. (2.12), we take

$$W(\xi,y,p) = X(\xi,p)e^{qy} \tag{2.14}$$

so that

$$A(\xi,p)W(\xi,y,p) = qW(\xi,y,p) \tag{2.15}$$

which leads to an eigenvalue problem. The characteristic equation corresponding to the matrix A is given by

$$\det[A - qI] = 0, \tag{2.16}$$

which on expansion leads to

$$q^6 - \lambda_1 q^4 + \lambda_2 q^2 - \lambda_3 = 0, \tag{2.17}$$

where

$$\begin{aligned} \lambda_1 &= Q_{15}Q_{24} + Q_{16}Q_{34} + Q_{11} + Q_{22} + Q_{33}, \\ \lambda_2 &= Q_{15}(Q_{24}Q_{33} - Q_{23}Q_{34}) + Q_{16}(Q_{22}Q_{34} - Q_{24}Q_{32}) \\ &\quad + Q_{11}Q_{22} + Q_{22}Q_{33} + Q_{11}Q_{33} - Q_{23}Q_{32}, \\ \lambda_3 &= Q_{11}(Q_{22}Q_{33} - Q_{23}Q_{32}). \end{aligned} \tag{2.18}$$

The roots of Eq. (2.17) are $\pm q_i, \quad i = 1, 2, 3.$

The eigenvalues of the matrix A are the roots of Eq. (2.17). We assume that real parts of q_i are positive. The eigen-vector $X(\xi)$ corresponding to the eigenvalues q_i can be determined by solving the homogeneous equation

$$[A - qI]X(\xi, p) = 0. \tag{2.19}$$

The set of eigenvectors $X_i(\xi, p), \quad (i = 1, 2, 3, 4, 5, 6)$ may be obtained as

$$X_i(\xi, p) = \begin{bmatrix} X_{i1}(\xi, p) \\ X_{i2}(\xi, p) \end{bmatrix}, \tag{2.20}$$

where

$$X_{i1}(\xi, p) = \begin{bmatrix} a_i q_i \\ b_i \\ 1 \end{bmatrix}, \quad X_{i2}(\xi, p) = \begin{bmatrix} a_i q_i^2 \\ b_i q_i \\ q_i \end{bmatrix}, \tag{2.21}$$

$$q = q_i \quad i = 1, 2, 3,$$

$$X_{j1}(\xi, p) = \begin{bmatrix} -a_i q_i \\ b_i \\ 1 \end{bmatrix}, \quad X_{j2}(\xi, p) = \begin{bmatrix} a_i q_i^2 \\ -b_i q_i \\ -q_i \end{bmatrix}, \tag{2.22}$$

$$j = i + 3, q = -q_i \quad i = 1, 2, 3,$$

$$a_i = (q_i^2 Q_{15} + Q_{16}Q_{32} - Q_{15}Q_{33})/\Delta_i,$$

$$b_i = [q_i^4 - q_i^2(Q_{16}Q_{34} + Q_{11} + Q_{33}) + Q_{11}Q_{33}]/\Delta_i, \tag{2.23}$$

$$\Delta_i = q_i^2(Q_{15}Q_{34} + Q_{32}) - Q_{32}Q_{11}, \qquad i = 1, 2, 3.$$

The solution of Eq. (12) is given by

$$W(\xi, y, p) = \sum_{i=1}^{3} [B_i X_i(\xi, p)\exp(\mathrm{q_i y}) + \mathrm{B_{i+3}X_{i+3}}(\xi, \mathrm{p})\exp(-\mathrm{q_i y})], \tag{2.24}$$

where $B_i (i = 1, 2, 3, 4, 5, 6)$ are arbitrary constants.

Equation (2.24) represents the solution of the general problem in the plane strain case of micropolar orthotropic elasticity by employing the eigenvalue approach, and therefore it can be applied to a broad class of problems in the domains of Laplace and Fourier transforms.

3. Application

In this section, the general solutions for displacement and stresses presented in Eq. (2.24) will be used to yield the response of a half-space subjected to a uniform traction distribution and to a point load. The constants B_i will be determined by imposing the proper boundary conditions. These constants, when substituted in Eq. (2.24), enable us to obtain the displacement and stress solutions in the Fourier and Laplace transformed (ξ, y, p) domain. The final solution in the original domain (x, y, t) is obtained by a numerical inversion of both transforms.

CASE 1. Load in normal direction: In the half-space, the load $F(x)$ is applied in normal direction at the origin of the co-ordinate system. For this loading case the boundary conditions are:

$$t_{22}(x, 0, t) = -F(x)\delta(t), \qquad t_{21}(x, 0, t) = 0, \qquad m_{23}(x, 0, t) = 0. \tag{3.1}$$

. **CASE 2.** Load in tangential direction: In the half-space, the load $F(x)$ is applied in tangential direction at the origin of the co-ordinate system. For this loading case the boundary conditions are:

$$t_{22}(x, 0, t) = 0, \qquad t_{21}(x, 0, t) = -F(x)\delta(t), \qquad m_{23}(x, 0, t) = 0. \tag{3.2}$$

It can be seen that six unknowns are to be determined in Eq. (2.24) and only three boundary conditions appear in each case. For the half-space the radition conditions implies outgoing waves with decreasing amplitudes in the positive y-direction. Therefore the radiation condition requires that $B_1 = B_2 = B_3 = 0$.

3.1. Influence functions

The method to obtain the half-space influence function, i.e., the solutions due to distributed loads applied at the half-space surface, is to set directly the distributed loads $F(x)$ in Eqs. (3.1) and (3.2). The Fourier transform w.r. to the pair (x, ξ) for the case of uniform strip load of amplitude F_o and width $2a$, applied at the origin of the coordinate system is :

$$\tilde{F}(\xi) = F_o \frac{2\sin(\xi a)}{\xi} \tag{3.3}$$

SUBCASE 1 (a). Load acting in normal direction. The solutions for this case due to the uniformly distributed load are obtained as

$$\tilde{u}_2(\xi, y, p) = b_1 B_4 e^{-q_1 y} + b_2 B_5 e^{-q_2 y} + b_3 B_6 e^{-q_3 y}, \tag{3.4}$$

$$\tilde{m}_{23}(\xi, y, p) = -\frac{K_1}{A_{11}}[q_1 B_4 e^{-q_1 y} + q_2 B_5 e^{-q_2 y} + q_3 B_6 e^{-q_3 y}], \tag{3.5}$$

$$\tilde{t}_{22}(\xi, y, p) = -[N_1 B_4 e^{-q_1 y} + N_2 B_5 e^{-q_2 y} + N_3 B_6 e^{-q_3 y}], \tag{3.6}$$

where

$$B_i = 2F_o(M_j q_k - M_k q_j)\sin(\xi a)/\xi\Delta; \tag{3.7}$$
$$i = 4,\ j = 2,\ k = 3; \quad i = 5,\ j = 3,\ k = 1; \quad i = 6,\ j = 1,\ k = 2.$$

and

$$M_i = [(-\iota\xi A_{78} b_i + A_{88} a_i q_i^2) A_{11} + K_1(A_{88} - A_{78})]/A_{11}^2,$$
$$N_i = (A_{22} b_i - \iota\xi A_{12} a_i) q_i / A_{11}; \quad i = 1, 2, 3, \tag{3.8}$$

$$\Delta = M_1(q_2 N_3 - q_3 N_2) + M_2(q_3 N_1 - q_1 N_3) + M_3(q_1 N_2 - q_2 N_1). \tag{3.9}$$

SUBCASE 2 (a). Load acting in tangential direction. The solutions for this case are obtained as in Eqs. (3.4)-(3.6) by changing the values of the constant

$$B_i = 2F_o(N_j q_k - N_k q_j)\sin(\xi a)/\xi\Delta; \tag{3.10}$$
$$i = 4,\ j = 2,\ k = 3; \quad i = 5,\ j = 3,\ k = 1; \quad i = 6,\ j = 1,\ k = 2.$$

3.2. Green's functions

To synthesize the Green functions, *i.e.* the displacement and stress solutions due to a point load described as the Dirac Delta $F(x) = F_o\delta(x)$, its Fourier transform with respect to the pair (x, ξ)

$$\tilde{F}(\xi) = F_o \tag{3.11}$$

must be used. The expressions for displacement and stresses may be obtained in the same way as Eqs. (3.4)-(3.6) by using the constants for the corresponding case.

SUBCASE 1 (b). Load acting in normal direction.

$$B_i = F_o(M_j q_k - M_k q_j)/\Delta; \tag{3.12}$$

$$i = 4,\ j = 2,\ k = 3; \quad i = 5,\ j = 3,\ k = 1; \quad i = 6,\ j = 1,\ k = 2.$$

SUBCASE 2 (b). Load acting in tangential direction.

$$B_i = F_o(N_j q_k - N_k q_j)/\Delta; \tag{3.13}$$

$$i = 4,\ j = 2,\ k = 3; \quad i = 5,\ j = 3,\ k = 1; \quad i = 6, j = 1, k = 2,$$

PARTICULAR CASES: Taking

$$A_{11} = A_{22} = \lambda + 2\mu + K, \quad A_{77} = A_{88} = \mu + K, \quad A_{12} = \lambda,$$

$$A_{78} = \mu, \quad B_{44} = B_{66} = \gamma, \quad -K_1 = K_2 = \chi/2 = K,$$

we obtain the corresponding expressions for the micropolar isotropic elastic medium.

4. Inversion of transforms

The transformed displacements and stresses (3.4)-(3.6) are functions of y, the parameters of Laplace and Fourier transforms p and ξ respectively, and hence they are of the form $\tilde{f}(\xi, y, p)$. To get the function $f(x, y, t)$ in the physical domain, first we invert the Fourier transform using

$$\begin{aligned} \bar{f}(x, y, p) &= \frac{1}{2\pi} \int_{-\infty}^{\infty} e^{-\iota\xi x} \tilde{f}(\xi, y, p) d\xi, \\ &= \frac{1}{\pi} \int_{0}^{\infty} \{\cos(\xi x) f_e - \iota \sin(\xi x) f_o\} d\xi, \end{aligned} \tag{4.1}$$

where f_e and f_o are even and odd parts of the function $\tilde{f}(\xi, y, p)$, respectively.

Thus, expression (4.1) gives us the Laplace transform $\bar{f}(x, y, p)$ of the function $f(x, y, t)$. Following HONIG and HIRDES [7], the Laplace transform function $\bar{f}(x, y, p)$ can be inverted to $f(x, y, t)$.

The last step is to evaluate the integral in Eq. (4.1). The method of evaluating this integral by PRESS *et.al.* [9], which involves the use of Romberg's integration with adaptive step size. This also uses the results of successive refinement of the extended trapezoidal rule, followed by extrapolation of the results to the limit when the step size tends to zero.

5. Numerical results and discussion

For numerical computations, we take the following values of the relevant parameters for the orthotropic micropolar solid:

$$A_{11} = 13.97 \times 10^{10}\text{dyne/cm}^2, \qquad A_{22} = 13.75 \times 10^{10}\text{dyne/cm}^2,$$

$$A_{77} = 3.0 \times 10^{10}\text{dyne/cm}^2, \qquad A_{88} = 3.2 \times 10^{10}\text{dyne/cm}^2,$$

$$A_{12} = 8.13 \times 10^{10}\text{dyne/cm}^2, \qquad A_{78} = 2.2 \times 10^{10}\text{dyne/cm}^2,$$

$$B_{44} = 0.056 \times 10^{10}\text{dyne}, \qquad B_{66} = 0.057 \times 10^{10}\text{dyne}.$$

For comparison with the micropolar isotropic solid, following GAUTHIER [6], we take the following values of relevent parameters for the case of aluminum epoxy composite as

$$\rho = 2.19\,\text{gm/cm}^3, \qquad \lambda = 7.59 \times 10^{10}\text{dyne/cm}^2,$$

$$\mu = 1.89 \times 10^{10}\text{dyne/cm}^2, \qquad K = 0.0149 \times 10^{10}\text{dyne/cm}^2,$$

$$\gamma = 0.0268 \times 10^{10}\text{dyne}, \qquad j = 0.00196\,\text{cm}^2.$$

The comparison of dimensionless normal displacement $U_2[= u_2/F_o]$, normal force stress $T_{22}[= t_{22}/F_o]$ and couple stress $M_{23}[= m_{23}/F_o]$, for a micropolar orthotropic solid (MOS) and micropolar isotropic solid (MIS) due to normal and tangential uniform strip load (USL), have been studied and shown in Figs. 1,..,6. The computations were carried out for three values of dimensionless time $t = 0.10, 0.20$ and $t = 0.50$ at $y = 1.0$ in the range $0 \leq x \leq 10$. The solid lines either without the center symbols or with the center symbols represent the variations for $t = 0.1$, whereas the dashed lines with or without center symbols represent the variations for $t = 0.2$ and large dashed lines with or without center symbols represent variations for $t = 0.5$. The curves without center symbol correspond to the case of MOS whereas those with center symbol correspond to the case of MIS. All results are obtained for one value of dimensionless width $a_o = \omega a/c_1 = 1$.

CASE 1. The comparison of normal displacement $U_2[= u_2/F_o]$, normal force stress $T_{22}[= t_{22}/F_o]$ and couple stress $M_{23}[= m_{23}/F_o]$, for micropolar orthotropic solid (MOS) and micropolar isotropic solid (MIS) were studied due to a normal USL and have been shown in Figs. 1, 2 and 3.

Figure 1 presents the variation of normal displacement U_2 with x due to a normal USL. The value of displacement U_2 for MOS have been magnified by multiplying with 10, for all three values of time. For the case of MIS, as the time t increases from 0.1 to 0.5, the values of U_2 decrease at initial range of

x whereas for the cases of MOS, the response of displacement with respect to time is reverse. At the point of application of the source the values for MOS are smaller than those for MIS due to USL. The behaviour of variation is oscillatory in the whole range for both the cases.

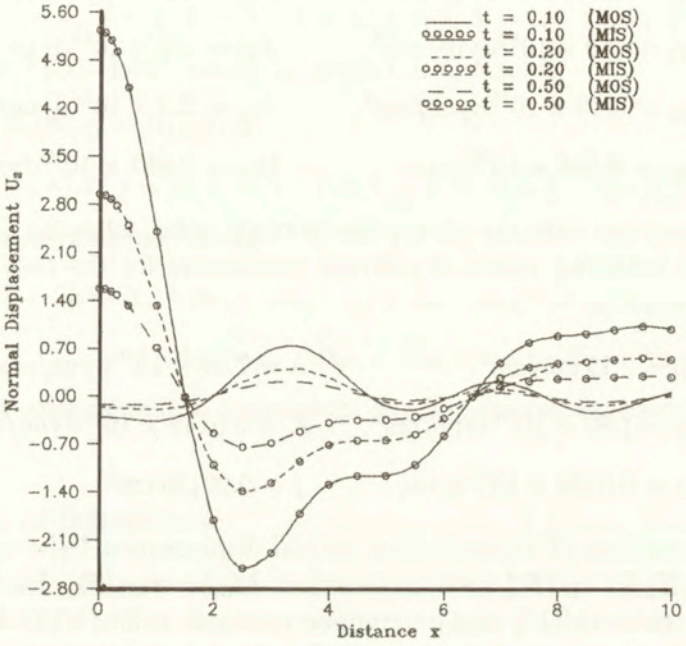

FIG. 1. Variation of normal displacement $U_2(x, 1, t)(= u_2/F_o)$ with distance x due to normal USL.

Figure 2 shows the variation of normal force stress T_{22} with x due to normal USL. The values of T_{22} for MOS have been multiplied by 10 for all three times. For all three times, the values of T_{22} for MIS are greater than the corresponding values for MOS at the point of application of the source. For MOS, initially, values of T_{22} start with a small decrease and then oscillate in further range, whereas for MIS values of stress initially decrease smoothly. For both MIS and MOS at the initial stage for the maximum value of time, the value of stress is maximum.

Figure 3 shows the variations of tangential couple stress M_{23} with x due to normal USL. For all three times and for the case of MOS, the value of M_{23} starts with a sharp decrease and than start to oscillate in the range $3 \leq x \leq 10$. For the case of MIS, the behaviour of variation of couple stress in time is reverse to that for MOS. As the range of x increases, the values of couple stress tend towards zero.

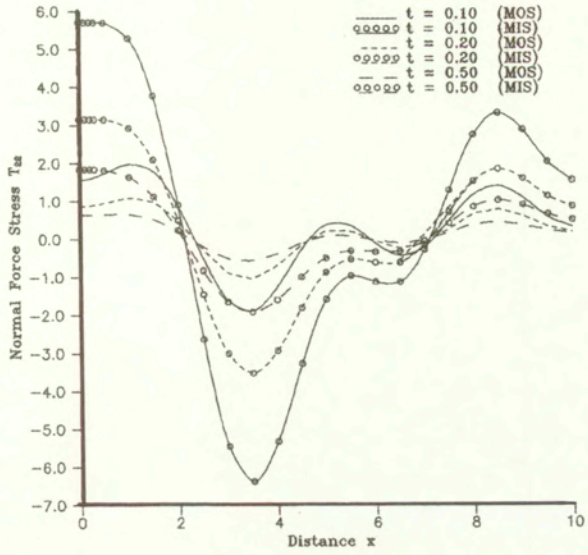

FIG. 2. Variation of normal force stress $T_{22}(x,1,t)(=t_{22}/F_o)$ with distance x due to normal USL.

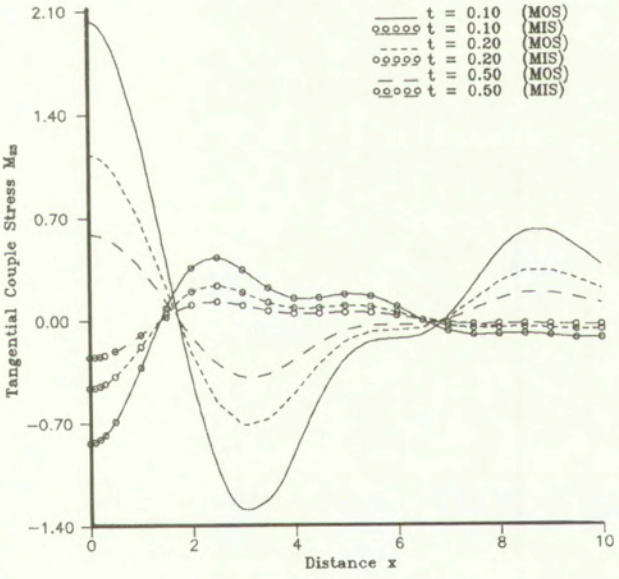

FIG. 3. Variation of tangential couple stress $M_{23}(x,1,t)(=m_{23}/F_o)$ with distance x due to normal USL.

CASE 2. Tangential Source: The comparison of normal displacement $U_2[=u_2/F_o]$, normal force stress $T_{22}[=t_{22}/F_o]$ and couple stress $M_{23}[=m_{23}/F_o]$, for

micropolar orthotropic solid (MOS) and micropolar isotopic solid (MIS) have been studied due to a tangential uniform strip load (USL), and have been shown in Figs. 4, 5 and 6. The values of U_2 and T_{22} for MOS are magnified by multiplying with 10 for all three times.

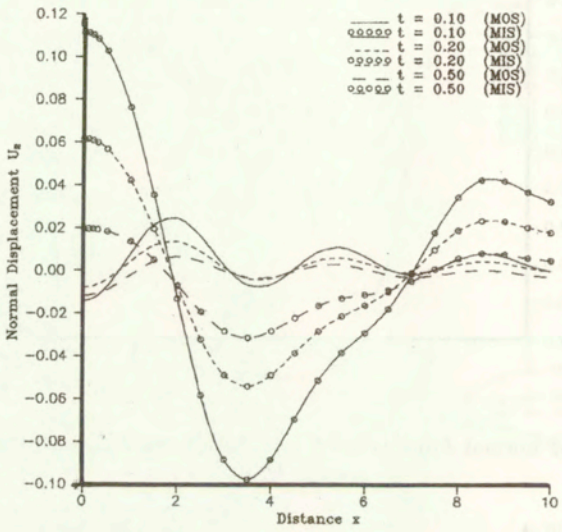

FIG. 4. Variation of normal displacement $U_2(x, 1, t)(= u_2/F_o)$ with distance x due to tangential USL.

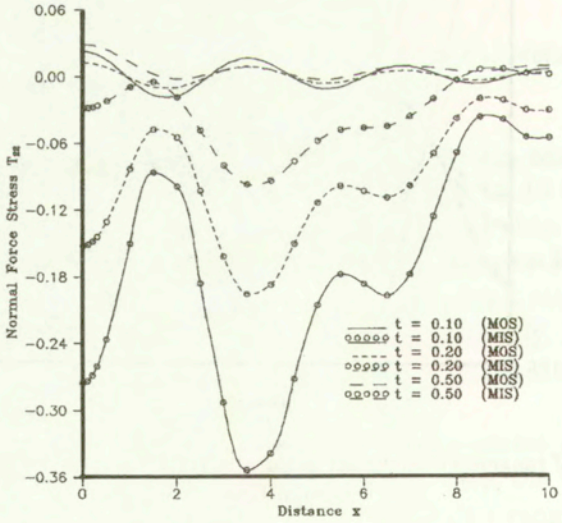

FIG. 5. Variation of normal force stress $T_{22}(x, 1, t)(= t_{22}/F_o)$ with distance x due to tangential USL.

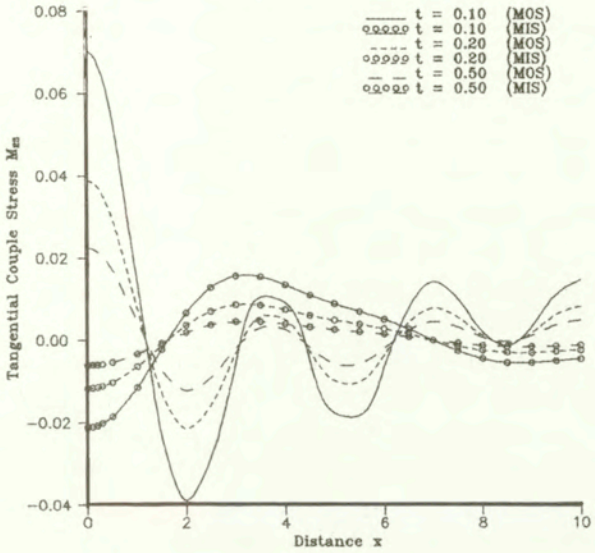

FIG. 6. Variation of tangential couple stress $M_{23}(x,1,t)(=m_{23}/F_o)$ with distance x due to tangential USL.

Figure 4 shows the variations of normal displacement U_2 with x due to tangential USL. The behaviour of variation of displacement is similar to that due to normal USL as in Fig. 1. However, their corresponding values are different.

Figure 5 shows the variation of normal force stress T_{22} with x due to tangential USL. The variation of stress for MOS is oscillating with smooth changes, whereas behaviour of variation for MIS is oscillating with greater changes. As the value of x increases the value for both the cases approaches zero.

Figure 6 shows the variation of tangential couple stress M_{23}. The variation of couple stress is similar to that due to normal USL, as in Fig. 3. However, their corresponding values are different.

6. Conclusion

A significant anisotropy effect is obtained in normal displacement, force stress and couple stress, for all values of time. Due to impulsive force, the character of solution is transient.

References

1. A. C. ERINGEN, *Linear theory of micropolar elasticity*, J. Math. Mech., **15**, 909-924, 1966.
2. A. C. ERINGEN, *Theory of micropolar elasticity in fracture, Vol II*, (Academic Press), 621-729, 1968.

3. D. IESAN, *The plane micropolar strain of orthotropic elastic solids,* Archives of Mechanics, **25**, 547-561, 1973.

4. D. IESAN, *Torsion of anisotropic elastic cylinders,* ZAMM , **54**, 773-779, 1974.

5. D. IESAN, *Bending of orthotropic micropolar elastic beams by terminal couples,* An. St. Uni. Iasi., **XX**, 411-418, 1974.

6. R. D. GAUTHIER, *In experimental investigations on micropolar media,* Mechanics of Micropolar Media, O. BRULIN and R. K. T. HSIEH [Ed.], World Scientific, Singapore, 1982.

7. G. HONIG and U. HIRDES, *A method for the numerical inversion of the Laplace transform,* J. Comp. Appl. Math., **10**, 113-132, 1984.

8. S. NAKAMURA, R. BENEDICT and R. LAKES, *Finite element method for orthotropic micropolar elasticity,* Int. J. Engng. Sci., **22**, 319-330, 1984.

9. W. H. PRESS, S. A. TEUKOLSKY, W. T. VELLERLIG and B. P FLANNERY, *Numerical recipes in FORTRAN,* (2^{nd} edition) Cambridge University Press, Cambridge, 1986.

10. R. K. MAHALABANABIS and J. MANNA, *Eigenvalue approach to linear micropolar elasticity,* Indian J. Pure Appl. Math., **20**, 1237-1250, 1989.

11. Z. Q. CHENG and L. H. HE, *Micropolar elastic field due to a spherical inclusion,* Int. J. Engng. Sci., **33**, 389-397, 1995.

12. Z. Q. CHENG and L. H. HE, *Micropolar elastic field due to a circular inclusion,* Int. J. Engng. Sci., **35**, 659-668, 1997.

13. R. K. MAHALABANABIS and J. MANNA, *Eigenvalue approach to the problem of linear micropolar thermoelasticity,* Indian Acad. Math. Sci., **19**, 69-86, 1997.

14. H. A. ERBAY, *An asymptotic theory of thin micropolar plates,* Int. J. Engng. Sci., **38**, 1497-1516, 2000.

15. R. KUMAR and S. DESWAL, *Steady-state response of a micropolar generalized thermoelastic half-space to the moving mechanical/thermal loads,* Proc. Indian Acad. (Math. Sci), **119**, 449-465, 2000.

16. R. KUMAR and S. DESWAL, *Mechanical and thermal source in a micropolar generalized thermoelastic medium,* Journal of Sound and Vibrations, **239** 467-488, 2001.

17. R. KUMAR, R. SING and T. K. CHADHA, *Eigenvalue approach to micropolar medium due to impulsive force at the origin,* Indian J. Pure Appl. Math., **32**, 1127-1144, 2001.

Received November 6, 2001; revised version March 3, 2002.

Arch. Mech., 54, 3, pp. 199–222, Warszawa 2002

Immersed boundary approach to stability equations for a spatially periodic viscous flow

J. SZUMBARSKI

Institute of Aeronautics and Applied Mechanics,
Warsaw University of Technology,
24 Nowowiejska St., 00-665 Warsaw

AN EFFICIENT NUMERICAL method for the linear stability equations of a spatially periodic channel flow is presented. The method is based on global Fourier-Chebyshev approximation of a disturbance velocity field. The physical flow domain is embedded in a larger computational domain and the boundary conditions are re-formulated as internal conditions imposed at immersed boundaries. The advantage of this approach is an avoidance of domain mapping, leading to tremendous complication of governing equations and to excessive computational cost. The results of numerical tests are presented. Favorable convergence properties with respect to the length of the Fourier expansions are demonstrated.

1. Introduction

DURING THE LAST two decades, a significant progress has been achieved in understanding the dynamics of instability and transition in many kinds of shear flows. A great deal of work in this area has been devoted to the analysis of parallel flows, like the Cuette flow, plane Poiseuille flow or flow in a pipe (Hagen-Poiseuille flow). The common feature of such flows is a very simple geometry of boundaries of the flow domain.

In the Ref. [1], FLORYAN investigated the problem of linear stability of shear flows in the presence of surface roughness. Actually, the boundary irregularities were "simulated" by a distributed surface transpiration. Thus, the flow boundaries were still straight lines and the author was able to apply directly a standard Fourier-Chebyshev method. In later works [2] and [3], the flow in a channel with corrugated walls has been investigated. The stability equations have been solved in a transformed computational space by a Chebyshev-collocation method. The transformation from the physical space (corrugated walls) to the computational space (straight walls) has generated, however, a tremendously complicated form of the governing equations. Most importantly, the stability equations in the transformed space could not be cast in the reduced form, i.e. the form involving only amplitude functions of the wall-normal velocity and vorticity components. Therefore, the algebraic eigenvalue problems solved in [2] or [3] were typically two or

more times larger than those for "simulated" roughness in [1], though using the same number of Fourier modes to the represent the disturbance fields. Consequently, the numerical difficulties in accurate determination of unstable modes have been encountered.

The objective of this paper is to propose an alternative approach. Working directly in a physical space gives an obvious advantage of dealing with a much simpler and smaller set of equations. However, the use of a spectral method based on global basic functions implies that the computational domain is a Cartesian product of two intervals, i.e. the ranges of variation of the streamwise and the wall-normal coordinate. Consequently, the computational domain of such a method is by default rectangular. On the other hand, the shape of the actual flow domain is not a rectangle – the lower and upper boundaries are wavy lines (although the magnitude of the wall corrugation is assumed to be rather small). Nevertheless, the formulation of the spectral method working directly in the physical space is indeed possible. In the Ref. [4], SZUMBARSKI and FLORYAN proposed a method based on the idea of immersed boundaries. The curvilinear physical domain is embedded in a rectangular computational domain. The physical boundaries of the flow (walls of a channel) are located in the interior of the computational domain and the conditions imposed on the velocity field at the channel walls are enforced as internal conditions. The objective of this paper is to demonstrate that the same approach can be used to obtain an effective and accurate solution method in the linear stability analysis.

The paper is organized as follows. In the Sec. 2, the problem of the basic flow determination is formulated mathematically and the numerical method is outlined. The presentation in that section follows closely the Ref. [4]. In the Sec. 3, the equations of linear stability are formulated. Section 4 is devoted to detailed description of the discretization of the stability equations using Chebyshev polynomials. Section 5 presents the major idea of the paper, i.e. the implementation of the original boundary conditions as the internal conditions in the extended computational domain. In the Sec. 6, the structure of the generalized eigenvalue problem obtained as a result of the spectral discretization is described. Finally, the results of the convergence tests are provided in the Sec. 7. Some additional technical issues are summarized in the Appendix.

2. Flow in a wavy channel

Consider the viscous flow in a plane channel with wavy boundaries. The walls can assume arbitrary shapes described by $y_L(x)$ and $y_U(x)$, where the subscript L refers to the bottom wall and the subscript U refers to the upper wall of the channel, respectively. The shape of the walls is assumed to be spatially periodic and thus the functions $y_L(x)$ and $y_U(x)$ can be expressed in the form of the

following Fourier expansions:

$$
\begin{aligned}
y_L(x) &= (A_0)_L + \frac{1}{2}\sum_{k=1}^{\infty}(A_k)_L \exp(ik\alpha x) + \frac{1}{2}\sum_{k=1}^{\infty}(A_k)_L^* \exp(-ik\alpha x,) \\
y_U(x) &= (A_0)_U + \frac{1}{2}\sum_{k=1}^{\infty}(A_k)_U \exp(ik\alpha x) + \frac{1}{2}\sum_{k=1}^{\infty}(A_k)_U^* \exp(-ik\alpha x)
\end{aligned}
\tag{2.1}
$$

where the wave number α characterizes the spatial period λ_x of the wall geometry, i.e. $\lambda_x = 2\pi/\alpha$. The coefficients $(\mathrm{A}_0)_L = -1$ and $(\mathrm{A}_0)_U = 1$ define y-coordinate of the middle lines of the wavy walls. The star superscript refers to the complex conjugation.

One can define the vertical extent of the flow domain as the interval $[Y_L, Y_U]$, where $Y_L = \min\limits_{x\in[0,\lambda_x]} y_L(x)$ and $Y_U = \max\limits_{x\in[0,\lambda_x]} y_U(x)$.

Since we are mostly interested in small or moderate magnitudes of wall waviness, it is reasonable to represent the velocity and pressure fields as the sums of the reference values, i.e. the values corresponding to the flow in a channel with straight boundaries (the Poiseuille flow)

$$
\begin{aligned}
\mathbf{V}_0(\mathbf{x}) &= [u_0(x,y)\,,\, v_0(x,y)] = [u_0(y)\,,\, 0] = \left[1-y^2,\, 0\right], \\
p_0(\mathbf{x}) &= -2\,x/\mathrm{Re}\ ,
\end{aligned}
\tag{2.2}
$$

and the modifications caused by the change of shapes of the boundaries, namely

$$
\begin{aligned}
\mathbf{V}_0(\mathbf{x}) &= [u(x,y),\, v(x,y)] = \mathbf{V}_0(\mathbf{x}) + \mathbf{V}_1(\mathbf{x}) \\
&= [u_0(y)\,,\, 0] + [u_1(x,y)\,, v_1(x,y)], \\
p(\mathbf{x}) &= p_0(\mathbf{x}) + p_1(\mathbf{x})\ .
\end{aligned}
\tag{2.3}
$$

It should be clear that for the wavy walls we have $Y_L < -1$ and $Y_U > 1$. Thus, the formula (2.3) involves evaluation of the reference velocity parabolic profile also at points located outside the original range [-1,1].

Substitution of the representation (2.3) of the flow quantities into the Navier-Stokes and continuity equations results in the following form of the governing equations:

$$
\begin{aligned}
u_0\,\partial_x u_1 + u_1\,\partial_x u_1 + v_1\,Du_0 + v_1\,\partial_y u_1 &= -\partial_x p_1 + \frac{1}{\mathrm{Re}}\left(\partial_{xx}u_1 + \partial_{yy}u_1\right), \\
u_0\,\partial_x v_1 + u_1\,\partial_x v_1 + v_1\,\partial_y v_1 &= -\partial_y p_1 + \frac{1}{\mathrm{Re}}\left(\partial_{xx}v_1 + \partial_{yy}v_1\right), \\
\partial_x u_1 + \partial_y v_1 &= 0,
\end{aligned}
\tag{2.4}
$$

where D stands for the differential operator d/dy, i.e. $Du_0 \equiv du_0/dy$. It is convenient to formulate the problem in terms of the stream function of the velocity modification defined as $u_1 = \partial_y \Psi$, $v_1 = -\partial_x \Psi$. The following equation can be derived:

$$(u_0 \partial_x + \partial_y \Psi\, \partial_x - \partial_x \Psi\, \partial_y)\ \Delta\Psi - D^2 u_0\, \partial_x \Psi = \frac{1}{\mathrm{Re}} \Delta^2 \Psi, \tag{2.5}$$

where Δ denotes the Laplace operator. Since u_1 and v_1 are periodic in x with the period $\lambda_x = 2\pi/\alpha$, the stream function can be represented as

$$\Psi(x,y) = \sum_{n=-\infty}^{n=+\infty} \Phi_n(y)\, e^{in\alpha x} \tag{2.6}$$

where $\Phi_n = \Phi^*_{-n}$ in order for Φ_n to be real. Inserting the expansion (2.6) into the Eq. (2.5), and separating the Fourier harmonics, the following system of the ordinary differential equations is obtained:

$$\begin{aligned} &\left[D_n^2 - in\alpha\, \mathrm{Re}\left(u_0 D_n - D^2 u_0\right)\right] \Phi_n \\ &\qquad - i\alpha\, \mathrm{Re} \sum_{k=-\infty}^{k=+\infty} \left[k\, D\Phi_{n-k} D_k \Phi_k - (n-k)\, \Phi_{n-k} D_k D\Phi_k\right] = 0, \end{aligned} \tag{2.7}$$

where $D_n = D^2 - n^2\alpha^2$. The boundary conditions at the channel walls are expressed in the following form:

$$\begin{aligned} &u_0(y_L(x)) + u_1(x, y_L(x)) = 0 \quad \text{and} \quad v_1(x, y_L(x)) = 0, \\ &u_0(y_U(x)) + u_1(x, y_U(x)) = 0 \quad \text{and} \quad v_1(x, y_U(x)) = 0. \end{aligned} \tag{2.8}$$

To obtain a complete formulation two additional conditions have to be imposed. The first one is simply the selection of the (constant) value of the stream function at one of the walls. The choice of the second is, in essence, arbitrary, but two possibilities are particularly important. We can prescribe the modification of the volume flux or the modification of the average pressure gradient along the channel. In this study, the first option is chosen and the additional conditions have the following form:

$$\begin{aligned} &\Psi_0(y_L(x)) + \Psi(x, y_L(x)) = 0, \\ &\Psi_0(y_U(x)) + \Psi(x, y_U(x)) = Q \ + q, \end{aligned} \tag{2.9}$$

where Ψ_0 denotes the stream function which corresponds to the reference flow, *i.e.* it is defined as $\Psi_0(y) = -\frac{2}{3} + y - \frac{1}{3}y^3$. Symbol Q denotes the volume flux

of the reference flow, namely

$$Q = \int_{-1}^{1} (1 - y^2)\, dy = \frac{4}{3},$$

while symbol q denotes the assumed modification of the volume flux. In the remaining part of the paper we assume that the flow in a wavy channel preserves the original volume flux, i.e. q = 0.

The numerical implementation of the conditions (2.8) and (2.9) is the key problem in the numerical solution of the system (2.7). In the remaining part of this section, we shall outline briefly the immersed boundary approach. Detailed description and testing of the method can be found in [4].

First, we define the computational domain to be a rectangular region spanning in y-coordinate from Y_L to Y_U. The extent of this region in x-coordinate is simply one spatial period λ_x. Thus, the physical domain is embedded in the computational one.

The next step is to represent the stream function in a form of truncated to N leading Fourier modes

$$\Psi(x, y) \approx \sum_{n=-N}^{n=N} \Phi_n(y)\ e^{in\alpha x}. \tag{2.10}$$

The formula (2.10) defines the stream function in the whole computational domain. Since the physical domain forms a proper subset of the computational one, the complement of the former is nonempty. In this area, the formula (2.10) defines a certain "fictitious" flow field.

The corresponding finite-dimensional system of the ordinary differential equations for the amplitude functions Φ_n, n=0,1,..,N is discretized by introducing Chebyshev representations of the unknown function Φ_n as follows:

$$\Phi_n(y) = \sum_{j=0}^{\infty} G_j^n T_j(y) \approx \sum_{j=0}^{J} G_j^n T_j(y)\,. \tag{2.11}$$

In the above formula, symbol T_j denotes the polynomial obtained as a results of composition of the j-th Chebyshev polynomial with the linear mapping transforming the interval $[Y_L, Y_U]$ into the interval [–1,1] (see Appendix A), and G_j^n stands for the unknown expansion coefficient. The Chebyshev representations of the required derivatives $D^l\Phi$ (with l up to l=4) can be determined using a differentiation algorithm (see [5], also the Appendix A).

The n-th equation of the system (2.7) can be written in a general form as

$$\Xi_n(\Phi_0, \Phi_1, .., \Phi_M) = 0 \quad \text{for} \quad n = 0, .., N. \tag{2.12}$$

The substitution of the Chebyshev expansions (2.11) and their derivatives into (2.12) gives the residual function

$$R_n = \Xi_n \left(\sum_{j=0}^{J} G_j^0 T_j, \sum_{j=0}^{J} G_j^1 T_j, .., \sum_{j=0}^{J} G_j^M T_j \right), \quad n = 0, .., N. \tag{2.13}$$

The problem is converted to an algebraic, nonlinear system by imposing the orthogonality conditions

$$\langle R_n, T_j \rangle_\omega = 0, \quad j = 0, .., J-4, \quad n = 0, .., N. \tag{2.14}$$

The inner product used in (2.14) is defined as follows:

$$\langle f, g \rangle_\omega := \int_{Y_L}^{Y_U} f(x)\, g(x)\, \omega(x)\, dx,$$

where the Chebyshev weight function ω, along with other useful formulas, is given in the Appendix A.

The discretization method described above can be viewed as a variant of the Chebyshev-tau technique. The reader should note that the projection (2.14) is carried out onto the linear subspace spanned by the Chebyshev polynomials with the order of up to $J-4$. The additional equations required to close the system are due to the flow boundary conditions (2.8) and the volume flux modification (2.9).

We shall describe briefly the treatment of the boundary conditions (a detailed exposition can be found in [4]). The idea is to derive explicitly the forms of the Fourier expansions of the velocity distribution along the wavy walls. Consider an arbitrary line $l := \{(x,y) : y = f(x)\}$ located entirely in the computational domain ($Y_L \leq f(x) \leq Y_U$), where the function f is periodic and it is expressed as

$$f(x) = f_0 + \tfrac{1}{2} \sum_{k=1}^{\infty} f_k \exp(ik\alpha x) + \tfrac{1}{2} \sum_{k=1}^{\infty} f_k^* \exp(-ik\alpha x.) \tag{2.15}$$

The velocity components, computed along the line l, are the x-periodic functions and thus they can be expressed in terms of Fourier series as

$$\begin{aligned} u_l(x) &\equiv u(x, f(x)) = \sum_{n=-\infty}^{+\infty} U_n\, e^{in\alpha x}, \\ v_l(x) &\equiv v(x, f(x)) = \sum_{n=-\infty}^{+\infty} V_n\, e^{in\alpha x}. \end{aligned} \tag{2.16}$$

On the other hand, the same distributions can be obtained with the use of the stream function, namely

$$u_l(x) \equiv u(x, f(x)) \cong u_0(f(x)) + \sum_{n=-N}^{N} D\Phi_n(f(x)) e^{in\alpha x}$$

$$= u_0(f(x)) + \sum_{n=-N}^{N} \sum_{j=0}^{J} G_j^n \, DT_j(f(x)) e^{in\alpha x},$$

(2.17)

$$v_l(x) \equiv v(x, f(x)) \cong -i\,\alpha \sum_{n=-N}^{N} n \, \Phi_n(f(x)) \, e^{in\alpha x}$$

$$= -i\,\alpha \sum_{n=-N}^{N} \sum_{j=0}^{J} n \, G_j^n T_j(f(x)) \, e^{in\alpha x}.$$

The need for the Fourier expansions of the Chebyshev polynomials and their first derivative is apparent. We can write

$$T_j(f(x)) = \sum_{k=-\infty}^{\infty} w_k^j e^{ik\alpha x}, \qquad DT_j(f(x)) = \sum_{k=-\infty}^{\infty} d_k^j e^{ik\alpha x}. \tag{2.18}$$

The expansion coefficients in (2.18) can be calculated, see Appendix A. Inserting (2.18) into (2.17), and comparing the obtained Fourier coefficients with the coefficients in (2.16), we obtain

$$U_n = F_n + \sum_{m=-N}^{N} \sum_{j=0}^{J} d_{n-m}^j G_j^m, \quad V_n = -i\alpha \sum_{m=-N}^{N} \sum_{j=0}^{J} m \, w_{n-m}^j G_j^m. \tag{2.19}$$

In the above formula, F_n denotes the Fourier coefficient of the function $u_0(f(x))$, i.e. the velocity of the reference flow computed along the line l.

The expressions (2.19) are the bases for implementation of the boundary conditions (2.8). It is necessary to apply them separately for each wall of the channel, i.e. to set $f(x) = y_L(x)$ and $f(x) = y_U(x)$. A minor complication arises, however. It has been shown in [4] that the value of the Fourier coefficient V_0 cannot be assumed independently. Instead, we have two equations corresponding to the volume flux conditions (2.9). The final form of the algebraic equation corresponding to (2.8) and (2.9) is the following:

$$(F_n)_{L,U} + \sum_{m=-N}^{N} \sum_{j=0}^{J} \left(d_{n-m}^j\right)_{L,U} G_j^m = 0, \qquad N \geq n \geq 0,$$

$$\sum_{m=-N}^{N}\sum_{j=0}^{J} m\left(w_{n-m}^{j}\right)_{L,U} G_j^m = 0\,, \quad N \geq n \geq 1\,,$$

$$(H_0)_L + \sum_{m=-N}^{N}\sum_{j=0}^{J} G_j^m (w_m^j)_L^* = 0\,,$$

(2.20)

$$(H_0)_U + \sum_{m=-N}^{N}\sum_{j=0}^{J} G_j^m (w_m^j)_U^* = Q + q\,,$$

where the subscripts L and U mean that the formulas are to be applied to the lower and the upper wall separately, $(H_0)_L$ and $(H_0)_U$ denote the coefficients of the zero Fourier mode of the functions $\Psi_0(y_L(x))$ and $\Psi_0(y_U(x))$. The precise meaning of the above equations is the following. The first group of the equations expresses the fact that $N+1$ leading Fourier modes of the boundary distribution of the x-components of the flow velocity must vanish. The second group of the equations plays the same role with respect to the y-component of the velocity field. As we have already mentioned, the equation for the zero Fourier mode is excluded, as it is actually satisfied automatically. The role of the two last equations is to set the average values of the complete (the reference flow and the modification) stream function at the channel boundaries.

The complete nonlinear system consists of the Eqs. (3.4) and (3.11). It can be written in a form including the complex Chebyshev coefficients of the amplitude function with only non-negative indices. Thus, its dimension is $(N+1)\cdot(K+1)$. It can be solved efficiently using an algorithm, which takes advantage of the particular structure of the equations. Such algorithm has been described in details in [4].

3. The equations of linear stability

The complete velocity field of the flow in the channel with wavy walls is x-periodic. For the sake of further convenience, the components of the velocity will be expressed as the following Fourier expansions

$$(3.1)\quad U(x,y) = \sum_{n=-\infty}^{\infty} F_U^n(y)\exp(in\alpha x), \quad V(x,y) = \sum_{n=-\infty}^{\infty} F_V^n(y)\exp(in\alpha x)\,.$$

Clearly, we have $F_U^{-n} = (F_U^n)^*$ and $F_V^{-n} = (F_V^n)^*$, since both functions in (3.1) are real.

The amplitude functions in (3.1) can be expressed in terms of the amplitude functions of the stream function, namely

$$
\begin{aligned}
&F_U^0(y) = u_0(y) + D\Phi_0(y), \quad F_U^n(y) \equiv \left(F_U^{-n}(y)\right)^* = D\Phi_D(y), \quad n > 0, \\
&F_V^n(y) \equiv \left(F_V^{-n}(y)\right)^* = -in\alpha\Phi_n(y), \quad n \geq 0\,.
\end{aligned} \tag{3.2}
$$

The linear analysis of stability of the flow defined by the formula (3.1) and (3.2) consists in investigation of the response of the flow to a small disturbance. Such analysis consists of four essential steps. In the first step, the class of admissible disturbances should be defined. Secondly, the equations governing the dynamics of admissible disturbances should be derived. As a result of this step, the eigenvalue differential problem is obtained. Thirdly, using appropriate discretization procedure, the differential problem has to be transformed to a tractable algebraic eigenvalue problem. Finally, the algebraic eigenvalue problem is to be solved in order to determine the most "dangerous" forms of disturbances, their amplification rates, critical Reynolds number and so on.

Since the main flow is x-periodic, the admissible form of a disturbance velocity field in the linear stability theory is

$$
\upsilon(t,x,y,z) = \sum_{m=-\infty}^{+\infty} \left[g_u^m(y), g_v^m(y), g_w^m(y)\right] \exp\left[i\left(t_m x + \beta z - \sigma t\right)\right] \tag{3.3}
$$

where $t_m = \delta + m\alpha$ and δ is a (real) Floquet exponent. Thus, the admissible disturbance is, in general, quasi-periodic in variable x.

Once the representation (3.3) is inserted into the linearized Navier-Stokes equations (in the velocity-vorticity formulation) and into the continuity equation then, after a rather lengthy algebra, the following equations are obtained:

$$
\begin{aligned}
S^m g_v^m = -\mathrm{Re}\sum_{n=1}^{\infty} \Big(& L_u^{m,n} g_u^{m-n} + L_v^{m,n} g_v^{m-n} + L_w^{m,n} g_w^{m-n} \\
& + M_u^{m,n} g_u^{m+n} + M_v^{m,n} g_v^{m+n} + M_w^{m,n} g_w^{m+n} \Big)\,,
\end{aligned}
$$

$$
\begin{aligned}
Q^m(t_m g_w^m - \beta g_u^m) + \mathrm{Re}\beta \cdot DF_u^0 g_v^m = i\mathrm{Re}\sum_{n=1}^{\infty} \Big(& N_u^{m,n} g_u^{m-n} + N_v^{m,n} g_v^{m-n} \\
& + N_w^{m,n} g_w^{m-n} + K_u^{m,n} g_u^{m+n} + K_v^{m,n} g_v^{m+n} + K_w^{m,n} g_w^{m+n} \Big)\,,
\end{aligned} \tag{3.4}
$$

$$
it_m g_u^m + Dg_v^m + i\beta g_w^m = 0, \quad m = .. -2, -1, 0, 1, 2, ...
$$

The left-hand side operators appearing in the Eq. (3.4) are defined as

$$
\begin{aligned}
S^m &= \left(D^2 - k_m^2\right)^2 - i\mathrm{Re}\left[\left(t_m F_u^0 - \sigma\right)\left(D^2 - k_m^2\right) - t_m D^2 F_u^0\right], \\
Q^m &= D^2 - k_m^2 - i\mathrm{Re}\left(t_m F_u^0 - \sigma\right),
\end{aligned} \tag{3.5}
$$

where $k_m^2 = t_m^2 + \beta^2$. The operators (3.5) can be regarded as generalizations of Orr-Sommerfeld and Squire operators. The operators in the right-hand side of the equations are rather complicated and we skip their explicit form. For the case $n = 1$, these operators have been presented by FLORYAN [1]. Besides, we will further transform the Eq. (3.4) to obtain a more tractable form.

It is well known that the equations of linear stability of a parallel flow can be converted into the equations for wall-normal components of velocity and vorticity fields of the disturbance flow. Similar procedure can be applied to the equations (3.4). The main advantage is the reduction of the number of unknowns and lowering the dimension of the algebraic eigenvalue problem obtained as a result of discretization of the system (3.4).

As a first step, the following functions are introduced

$$\theta^m(y) = t_m g_w^m(y) - \beta g_u^m(y), \quad m = .. -2, -1, 0, 1, 2, .. . \tag{3.6}$$

Then, using the definition (3.6) and the spectral form of the continuity equation

$$i\, t_m\, g_u^m(y) + D g_v^m + i\,\beta\, g_w^m = 0\,, \quad m = .. -2, -1, 0, 1, 2, .. \,,$$

the inverse relations can be derived

$$g_u^m = (i\, t_m D g_v^m - \beta\, \theta^m)\, /k_m^2, \quad g_w^m = (i\,\beta D g_v^m + t_m\, \theta^m)\, /k_m^2\,. \tag{3.7}$$

The reader should notice that θ^m is closely related to the Fourier representation of the y-components of the disturbance vorticity field $\boldsymbol{\upsilon}$. Indeed, one has

$$\omega_y = \partial_z \upsilon_x - \partial_x \upsilon_z = \sum_{n=-\infty}^{\infty} i\,(\beta g_u^n - t_m g_w^n) \exp\left[i\,(t_n x + \beta z - \sigma t)\right] \tag{3.8}$$

$$= -i \sum_{n=-\infty}^{\infty} \theta^n \exp\left[i\,(t_n x + \beta z - \sigma t)\right].$$

The stability equations expressed in terms of the amplitude functions $\{g_v^n,\ \theta^n\}$ assume the following form:

$$S^m g_v^m + \sum_{n=1}^{\infty} \left(\bar{G}_v^{m,n} g_v^{m+n} + G_v^{m,n} g_v^{m-n} + \bar{G}_\theta^{m,n} \theta^{m+n} + G_\theta^{m,n} \theta^{m-n}\right) = 0$$

$$m = .., -2, -1, 0, 1, 2, ..$$

(3.9)

$$Q^m \theta^m + \mathrm{Re}\beta\, D F_u^0 g_v^m$$

$$+ \sum_{n=1}^{\infty} \left(\overline{E}_v^{m,n} g_v^{m+n} + E_v^{m,n} g_v^{m-n} + \overline{E}_\theta^{m,n} \theta^{m+n} + E_\theta^{m,n} \theta^{m-n}\right) = 0.$$

In the above, the operators S^m and Q^m are defined as previously by (3.5). The expressions of the other operators are rather long and therefore they are presented the Appendix B.

The disturbance velocity field should vanish at the boundaries of the flow domain. Thus, the Eq. (3.9) are supplemented by homogeneous boundary conditions imposed at the wavy walls of the channel. It will be explained in Sec. 5 how the treatment of the boundary conditions applied for the main flow in Sec. 2 can be adopted in the stability analysis.

4. The numerical method for the stability equations

4.1. Spectral discretization of the stability equations

The structure of the set of the stability Eq. (3.9) is simple – for each integral number we have a pair of two differential equations, the first of the fourth order and the other of the second order. Clearly, all these pairs of the equations are coupled. Supplemented by appropriate homogeneous boundary conditions, the Eq. (3.9) define the eigenvalue problem. Nontrivial solutions can exist only for certain combinations of the following parameters: the Reynolds number Re, wave numbers α and β, the Floquet exponent δ and the complex amplification rate σ. In the analysis of temporal stability, we are interested in determination of the amplification rate σ as a function of the remaining parameters. Mathematically, a linear differential eigenvalue problem must be solved. After suitable discretization and truncation, a finite-dimensional algebraic problem is obtained. It can be solved numerically with the use of standard tools, for instance those from the LAPACK library.

The numerical method used to solve the stability equations can be regarded as a variant of the spectral Chebyshev-Galerkin method. The unknown amplitude functions are sought in the form of (truncated) Chebyshev expansions

$$g_v^n(y) = \sum_{k=0}^{K_V} \Gamma_k^n T_k(y), \quad \theta^n(y) = \sum_{k=0}^{K_\theta} \Theta_k^n T_k(y). \tag{4.1}$$

As in the Sec. 2, the Chebyshev polynomials are defined on the interval $[Y_L, Y_U]$. The further procedure consists in three steps:

1. Insertion of the above expansions into the stability equations.
2. Projection of the equations obtained after the first step onto the subspace spanned by a finite number of the Chebyshev polynomials. For each fourth-order equation, the projection is made by computing the weighted inner products with the functions $T_0, T_1, .., T_{K_V-4}$. For each second-order equation the projection is made by computing the weighted inner products with the polynomials $T_0, T_1, .., T_{K_\theta-2}$. The additional six equations (for

each fourth/second-order pair) come from the direct enforcement of the homogeneous boundary conditions.

3. Truncation of the originally infinite set of the stability equations to its finite-dimensional approximation. It means that in the computations, the range of the summation index "m" in the expansion (3.3) will be $-M, .., M$.

We first consider the discretization of the m-th fourth-order equation in (3.9) After the Chebyshev representations are inserted and the projections are made, one has

$$(4.2)\quad \sum_{k=0}^{K_V} \langle S^m T_k, T_j \rangle_\omega \Gamma_k^m + \sum_{n=1}^{\infty} \left\{ \sum_{k=0}^{K_V} \langle \bar{G}_V^{m,n} T_k, T_j \rangle_\omega \Gamma_k^{m+n} + \sum_{k=0}^{K_V} \langle G_V^{m,n} T_k, T_j \rangle_\omega \Gamma_k^{m-n} \right\} + \sum_{n=1}^{\infty} \left\{ \sum_{k=0}^{K_\theta} \langle \bar{G}_\theta^{m,n} T_k, T_j \rangle_\omega \Theta_k^{m+n} + \sum_{k=0}^{K_\theta} \langle G_\theta^{m,n} T_k, T_j \rangle_\omega \Theta_k^{m-n} \right\} = 0$$

$$j = 0, .., K_V - 4$$

where the inner product $\langle \cdot, \cdot \rangle_\omega$ is defined as described in the Appendix A.

Analogous procedure applied to the m-th second-order Eq. (3.9) yields

$$(4.3)\quad \sum_{k=0}^{K_\theta} \langle Q^m T_k, T_j \rangle_\omega \Theta_k^m + \beta \mathrm{Re} \cdot \sum_{k=0}^{K_V} \langle DF_u^0 T_k, T_j \rangle_\omega \Gamma_k^m + \sum_{n=1}^{\infty} \left\{ \sum_{k=0}^{K_V} \langle E_V^{m,n} T_k, T_j \rangle_\omega \Gamma_k^{m-n} + \sum_{k=0}^{K_V} \langle \bar{E}_V^{m,n} T_k, T_j \rangle_\omega \Gamma_k^{m+n} \right\} + \sum_{n=1}^{\infty} \left\{ \sum_{k=0}^{K_\theta} \langle E_\theta^{m,n} T_k, T_j \rangle_\omega \Theta_k^{m-n} + \sum_{k=0}^{K_\theta} \langle \bar{E}_\theta^{m,n} T_k, T_j \rangle_\omega \Theta_k^{m+n} \right\} = 0,$$

$$j = 0, .., K_\theta - 2.$$

Insertion of the explicit forms of all operators (see Appendix B) into the formulas (4.2) and (4.3) leads to rather complicated expressions. However, all of them can be computed in terms of seventeen elemental structures with two or three indices. Each entry of a double-index structure is defined by the Chebyshev integral of the products of a Chebyshev polynomial and an even-order derivative (up to 4^{th} order) of another one. Each entry of a triple-index structure is defined

by the Chebyshev integral of the product of a Chebyshev polynomial, a derivative (up to 3rd order) of another one, and one of the amplitude functions defined in (3.2) or one of its derivatives (up to 2nd order).

4.2. Numerical implementation of the boundary conditions

Main feature of the numerical method applied for the determination of the main flow is that the computational domain is extended to overlap the interior of the channel with wavy walls. Consequently, the basic functions for spectral expansions are the Chebyshev polynomials defined in the non-standard interval $[Y_L, Y_U]$. The boundary conditions at the channel walls are enforced as the internal conditions imposed along the wavy lines immersed in the interior of the extended computational domain.

The same technique can be applied to the homogeneous boundary conditions formulated for the disturbance velocity field in the stability analysis.

The derivation of the boundary conditions for the disturbance velocity field consists in four steps:

1. Derivation of the Fourier representation of the disturbance velocity distributions along the wavy walls.
2. Extracting the Fourier coefficients and setting them to zero.
3. Re-writing the obtained expressions in terms of the expansion coefficients of the amplitude functions g_V^m and θ^m.
4. Truncating to a finite number of Fourier modes in order to get the final computable form.

The derivation procedure will be demonstrated on the example of the y-component v_y computed for the bottom wall $y = y_L(x)$. The distribution along the bottom wall can be expressed as

$$
\begin{aligned}
(4.4)\quad v_y(x, y_L(x), z) &= \sum_{n=-\infty}^{\infty} g_V^n(y_b(x)) \exp\left[i\left(t_n x + \beta z - \sigma t\right)\right] \\
&= \sum_{n=-\infty}^{\infty} \left[\sum_{k=-\infty}^{\infty} \left(\sum_{j=0}^{\infty} \left(w_k^j\right)_L \Gamma_j^n \right) \exp\left(ik\alpha x\right) \right] \exp\left[i\left(t_n x + \beta z - \sigma t\right)\right] \\
&= \sum_{m=-\infty}^{\infty} \left[\sum_{n=-\infty}^{\infty} \left(\sum_{j=0}^{\infty} \left(w_{m-n}^j\right)_L \Gamma_j^n \right) \right] \exp\left[i\left(t_m x + \beta z - \sigma t\right)\right].
\end{aligned}
$$

Let us rewrite (4.4) in the following form

$$(4.5)\quad v_y(x, y_L(x), z)\exp\left[-i\left(\delta x+\beta z\right)\right]\exp\left(i\sigma t\right) = \sum_{m=-\infty}^{\infty}\left[\sum_{n=-\infty}^{\infty}\left(\sum_{j=0}^{\infty}\left(w_{m-n}^{j}\right)_L\Gamma_j^n\right)\right]\exp\left(i\,m\alpha x\right).$$

If we set all Fourier coefficients in right-hand side of (4.5) to zero then, at any time instant, the y-component of the disturbance velocity field will satisfy the homogeneous boundary condition at the bottom wall. Indeed, both the Floquet exponent δ and the spanwise wave number β are real, so the factor $\exp[-i(\delta x+\beta z)]$ is bounded in space. Thus, the second step of the derivation procedure yields

$$(4.6)\qquad \sum_{n=-\infty}^{\infty}\left(\sum_{j=0}^{\infty}\left(w_{m-n}^{j}\right)_L\Gamma_j^n\right)=0,\quad m=..-2.-1,0,1,2,...$$

Similar two equations are obtained for the remaining velocity components. Then, replacing the subscript "L" with "U" gives an analogous triple of equations for the upper wall.

In the third step, the conditions for the components v_x and v_z have to be expressed in terms of the functions g_V^m and θ^m. Using the relation (3.7), we end up with following formulas:

$$\sum_{n=-\infty}^{\infty}\left(\frac{it_n}{k_n^2}\sum_{k=1}^{\infty}\left(d_{m-n}^{k}\right)_L\Gamma_k^n-\frac{\beta}{k_n^2}\sum_{k=0}^{\infty}\left(w_{m-n}^{k}\right)_L\Theta_k^n\right)=0,$$

$$m=..,-2,-1,0,1,2,..$$

$$(4.7)\qquad \sum_{n=-\infty}^{\infty}\left(\frac{i\beta}{k_n^2}\sum_{k=1}^{\infty}\left(d_{m-n}^{k}\right)_L\Gamma_k^n+\frac{t_n}{k_n^2}\sum_{k=0}^{\infty}\left(w_{m-n}^{k}\right)_L\Theta_k^n\right)=0,$$

$$m=..,-2,-1,0,1,2,..$$

for the bottom wall. Again, a pair of analogous conditions for the upper wall is obtained by replacing the subscript "L" with "U".

This way, we obtain three additional homogeneous equations for each wall and each number (Fourier mode number) "m". To make finite computations possible, all sums in above expressions have to be truncated. The final form of

the equations expressing the boundary conditions at the channel walls is

$$\sum_{n=-M}^{M}\left(\sum_{k=0}^{K_V}\left(w^k_{m-n}\right)_{L,U}\Gamma^n_k\right)=0, \qquad m=-M,..,0,..,M,$$

$$\sum_{n=-M}^{M}\left(\frac{it_n}{k_n^2}\sum_{k=1}^{K_V}\left(d^k_{m-n}\right)_{L,U}\Gamma^n_k-\frac{\beta}{k_n^2}\sum_{k=0}^{K_\theta}\left(w^k_{m-n}\right)_{L,U}\Theta^n_k\right)=0, \tag{4.8}$$

$$m=-M,..,0,..,M,$$

$$\sum_{n=-M}^{M}\left(\frac{i\beta}{k_n^2}\sum_{k=1}^{K_V}\left(d^k_{m-n}\right)_{L,U}\Gamma^n_k+\frac{t_n}{k_n^2}\sum_{k=0}^{K_\theta}\left(w^k_{m-n}\right)_{L,U}\Theta^n_k\right)=0$$

$$m=-M,..,0,..,M.$$

In the above formula, the subscripts "L" and "U" refer to the bottom and upper walls, respectively.

4.3. Structure of the algebraic eigenvalue problem

The unknowns can be collected in the following block vector

$$\mathbf{z}=\left[\left\{\Gamma^n_0,\Gamma^n_1,..,\Gamma^n_{K_V-1},\Gamma^n_{K_V};\Theta^n_0,\Theta^n_1,..,\Theta^n_{K_\theta-1},\Theta^n_{K_\theta}\right\}, \tag{4.9}$$

$$n=-M,..,0,..M\right]^T.$$

Then, Eqs. (4.2), (4.3) and (4.8) can be written in the form of the homogeneous linear system

$$\mathbf{P}\cdot z=0. \tag{4.10}$$

The matrix $\mathbf{P}$ has a block structure. The block dimension of $\mathbf{P}$ is 2*M+1. All blocks are matrices with dimension $K_V+K_\theta+2$. The position of a block inside the matrix $\mathbf{P}$ can be described with the use of two block indices: row index m and the column index n. The range of these indices is $[-M,..,M]$. Each block with the row index m consists of K_V-3 rows corresponding to the m-th Eq. (4.2), $K_\theta-1$ rows corresponding to the m-th Eq. (4.3) and six rows corresponding to the m-th Eq. (4.8) enforcing the homogeneous boundary conditions.

The eigenvalue problem is defined by the characteristic equations for the homogeneous system, i.e. $\det\mathbf{P}=0$. In the case of temporal stability, one seeks the amplification exponent σ as a function of other parameters of the problem. In

such a case the eigenvalue problem is linear and can be expressed in the standard form as

$$\mathbf{P}_0 z = \sigma \mathbf{P}_1 z. \tag{4.11}$$

The matrices defining the generalized eigenvalue problem (4.11) can be obtained directly by extracting those parts of the stability equations, which do not contain σ. Alternatively, the matrix $\mathbf{P}$ can be considered as a function of the attenuation exponent σ and then the matrices in (4.11) can be determined as follows:

$$\mathbf{P}_0 = \mathbf{P}(0), \quad \mathbf{P}_1 = \mathbf{P}_0 - \mathbf{P}(1). \tag{4.12}$$

The generalized eigenvalue problem (4.11) can be solved using standard routines from the LAPACK library. However, the investigation of variations of selected eigenvalues/eigenvectors with a change of various parameters (Reynolds number, roughness geometry, wave numbers etc.) necessitates an efficient tracing algorithm. It seems that the **I**nverse **I**terations **M**ethod provides an appropriate tool for this task. The IIM can also be used to improve the accuracy of particular eigensolutions obtained by other methods. Although an exposition of this method can be found in many textbooks on the numerical algebra, for the sake of completeness it is presented in the Appendix C.

5. The convergence tests

In this section, we present results of the convergence tests. The numerical computations have been carried out for the Reynolds number Re=5000 and the wave numbers α=3 and β=2. The shape of the channel walls is assumed in the following form:

$$y_L(x) = -1 - S\cos(\alpha x), \quad y_U(x) = 1 + S\cos(\alpha x) \ ,$$

where S=0.02. The main flow is computed using fifteen Fourier modes (N=14) and sixty (J=59) Chebyshev polynomials per each amplitude function Φ_n. The assumed length of the Fourier representation of the main flow ensures that the error in enforcement of the boundary conditions (2.8) is less than 10^{-12}. The convergence test has been designed in the following way. For the flow parameters chosen for the test, two unstable modes exist: the Squire mode (Sq) and the Orr-Sommerfeld mode (OS). This situation is analogous to the case of distributed wall suction, discussed by the author in [6]. The corresponding eigenvalues are evaluated using different number of modes M in the disturbance Fourier expansion (3.3). With increasing number of modes, the representation of the disturbance

is getting more accurate. We also assume that the number of Fourier modes of the main flow accounted for in the stability computations is the largest possible, i.e. it is equal to M.

When the number of modes M increases, the convergence is expected. The computations are repeated with a different number of the Chebyshev polynomials. This way the convergence with respect to K_v and K_θ can be established as well. The latter issue is, however, less important because the efficiency of immersed boundary approach to the boundary conditions depends mostly on the convergence properties with respect to the Fourier expansions.

The results of the test computations are presented in Table 1. Rapid convergence of the evaluated eigenvalues is observed. Surprisingly enough, the computed values are quite accurate even for M=3. The values for M=7 and M=8 match to within nine significant digits. In the numerical stability analysis, such accuracy is more than satisfactory.

Table 1. The unstable eigenvalues computed for different values of the Fourier modes M and Chebyshev polynomials K_v and K_θ.

M	$\sigma \cdot 10^3$	$K_v = K_\theta$=49	$K_v = 59, K_\theta$=49	$K_v = K_\theta$=59
3	Sq	1.923180264	1.923152536	1.923125632
	OS	1.382477688	1.382428066	1.382420663
4	Sq	1.922667419	1.922629066	1.922598856
	OS	1.381969904	1.381912186	1.381896911
5	Sq	1.922661537	1.922622306	1.922592749
	OS	1.381965322	1.381907517	1.381891484
6	Sq	1.922662554	1.922623455	1.922593912
	OS	1.381966101	1.381908421	1.381892490
7	Sq	1.922662452	1.922623367	1.922593787
	OS	1.381966016	1.381908339	1.381892384
8	Sq	1.922662449	1.922623364	1.922593784
	OS	1.381966013	1.381908337	1.381892378

Practically, $M = 4$ or $M = 5$ is sufficient to obtain very good approximations of the leading eigenvalues. If one is interested in the corresponding eigensolutions, the accuracy of the boundary conditions should be also considered. It is instructive to compute the error in the boundary conditions for the components of the disturbance velocity field. Obviously, the value of the error is meaningful providing that an eigensolution is normalized. Table 2 shows the maximum norm of the boundary error computed at the bottom wall for the x-component of the disturbance velocity field. The latter is normalized so that its maximal value in the flow domain is the unity. The accuracy of the boundary conditions is im-

proving with increasing number of the Fourier modes. In the number of modes is sufficiently large, addition of one mode reduces the norm of the error by a certain factor, i.e. the error diminishes at exponential or spectral rate. The observed rate of convergence can be roughly characterized as reduction by two orders of the magnitude per each three more modes.

Table 2. The maximal boundary error of the velocity component v_x of the eigensolutions computed using different number of the Fourier modes. The number of the Chebyshev polynomials is $K_v = K_\theta = 59$.

M	3	4	5	6	7	8
Sq	$1.4767 \cdot 10^{-3}$	$3.2391 \cdot 10^{-4}$	$1.1662 \cdot 10^{-4}$	$3.1286 \cdot 10^{-5}$	$6.8561 \cdot 10^{-6}$	$1.5373 \cdot 10^{-6}$
OS	$1.4590 \cdot 10^{-3}$	$3.5159 \cdot 10^{-4}$	$1.2026 \cdot 10^{-4}$	$3.2257 \cdot 10^{-5}$	$7.0622 \cdot 10^{-6}$	$1.5943 \cdot 10^{-6}$

6. Concluding remarks

The numerical method described above offers an efficient alternative for the traditional approach based of the domain transformation. The technique of immersed boundaries seems to be particularly useful when the magnitude of boundary corrugation is sufficiently small, i.e. it is not larger than several percent of the channel width. This range of values it exactly what one would reasonably call the "wall roughness". The methods based on a domain transformation are not much competitive here, because of the "overhead" due to extreme complication of the stability equations in the computational domain. Another possibility is to resort to domain perturbation methods (DPM). The idea is to transfer the boundary conditions from a corrugated boundary to a straight centerline, and get an approximate form of boundary conditions with the use of a Taylor expansion of a certain order. First-order procedure is well described in [7]. The applicability of this approach to flows in a corrugated channel has been recently investigated by CABAL *et al.* [8] and compared with the domain transformation and immersed boundary techniques. The essential conclusion is that the DPM (even of higher orders) cannot provide a sufficient accuracy in enforcement of the boundary conditions, particularly when the magnitude of wall corrugation becomes sufficiently large for flow destabilization. Thus, it is rather unlikely that DPM applied to the stability problem considered here would be of any use.

There are, certainly, some limitations of efficiency or even applicability of the immersed boundary method. The magnitude of a corrugation has been already mentioned. The other problem is posed by large values of the wave numbers. It has been shown in [4] that computations with large values of the wave number α require much larger numbers of the Fourier modes and Chebyshev polynomials.

At the same time, the rate of convergence, although exponential, becomes much slower. Consequently, the overall efficiency of the methods significantly drops and the computational cost becomes prohibitive. For such extreme cases, the method based on the domain transformation, although much more complicated in derivation and implementation, would be a better option (see [7]). On the other hand, the wave numbers characterizing unstable forms of disturbances turn out to fall within the range of small or moderate values (α,β<10), where the immersed boundary approach is preferable.

Appendix A. Basic functions

Assume that the computational domain is the interval $[Y_L, Y_U]$. The transformation from the computational domain to the standard domain, i.e. the interval [–1,1], is given as

$$[Y_L, Y_U] \ni y \longrightarrow \eta(y) = p \cdot y + q \in [-1, 1] \tag{A.1}$$

where
$p = 2/(Y_U - Y_L)$ and $q = -(Y_L + Y_U)/(Y_U - Y_L)$.
The following set of functions (polynomials) can be defined

$$T_j(y) = t_j(p \cdot y + q), \quad j = 0, 1, 2.., \tag{A.2}$$

where t_j denotes the standard Chebyshev polynomial.

If the following weight function is introduced

$$\omega(y) = \Omega(p \cdot y + q), \quad \Omega(\eta) = \left(1 - \eta^2\right)^{-\frac{1}{2}} \tag{A.3}$$

then the functions defined by (A. 2) satisfy an orthogonality condition, namely

$$\int_{Y_L}^{Y_U} T_j(y)\, T_k(y) \omega(y)\, dy = \frac{1}{p} \int_{-1}^{1} t_j(\eta)\, t_k(\eta)\, \Omega(\eta)\, d\eta = \frac{1}{p} \begin{cases} 0 & \text{if } j \neq k, \\ \pi & \text{if } j = k = 0, \\ \pi/2 & \text{if } j = k > 0. \end{cases} \tag{A.4}$$

The derivative of the basic function T_j can be expressed in terms of the functions $T_0, T_1, .., T_{j-1}$ as follows:

$$DT_j(y) = \sum_{k=0}^{j-1} c_j^k \cdot T_k(y). \tag{A.5}$$

The expansion coefficients in (A.5) are related to the coefficients in Chebyshev differentiation formulae

$$Dt_j(\eta) = \sum_{k=0}^{j-1} C_j^k \cdot t_k(\eta), \tag{A.6}$$

namely, we have $c_j^k = p\, C_j^k$. The coefficients $\left\{ C_j^k \right\}$ are the following:

$$C_j^k = \begin{cases} 2j, & k \quad \text{is odd} \\ 0, & k \quad \text{is even} \end{cases} \qquad \text{– when } j \text{ is an even number,}$$

$$C_j^k = \begin{cases} 0, & k \quad \text{is odd,} \\ 2j, & k > 0 \text{ and even} \\ j, & k = 0. \end{cases} \qquad \text{– when } j \text{ is an odd number,}$$

The multiplication rule for the basic functions $\{T_j\}$ is the same as for the standard Chebyshev polynomials, i.e.

$$T_j \cdot T_k = \frac{1}{2} T_{j+k} + \frac{1}{2} T_{|j-k|}. \tag{A.7}$$

Another important operation is an inner product of a pair of the expansions in $\{T_j\}$. Consider two functions given as follows:

$$g(y) = \sum_{j=0}^{M} g_j T_j(y), \quad h(y) = \sum_{k=0}^{N} h_k T_k(y) \, .$$

Then the inner product is defined as follows:

$$\int_{Y_L}^{Y_U} g(y)\, h(y)\, \omega(y)\, dy = \frac{\pi}{p} \left(g_0 h_0 + \frac{1}{2} \sum_{k=1}^{\min(M,N)} g_k h_k \right) . \tag{A.8}$$

Implementation of the boundary conditions in the channel with wavy walls requires computations of the Fourier expansions of the following composite functions:

$$T_j(f(x)) = \sum_{k=-\infty}^{k=+\infty} w_k^j \exp(ik\alpha x), \quad DT_j(f(x)) = \sum_{k=-\infty}^{k=+\infty} d_k^j \exp(ik\alpha x) \, .$$

Since the basic functions are real, the coefficients satisfy obvious relations

$$w^j_{-k} = \left(w^j_k\right)^*, \quad d^j_{-k} = \left(d^j_k\right)^*, \quad k = 0, 1, .., \quad j = 0, 1, ...$$

The real function f is assumed in the form of the following Fourier series:

$$f(x) = f_0 + \frac{1}{2}\sum_{k=1}^{\infty} f_k \exp(ik\alpha x) + \frac{1}{2}\sum_{k=1}^{\infty} f^*_k \exp(-ik\alpha x)\,.$$

Using the recursive definition of the Chebyshev polynomials, one arrives at the following formulas:

$$\begin{aligned} w^{j+1}_k &= p\left(\sum_{n=0}^{\infty} f_n w^j_{k-n} + \sum_{n=0}^{\infty} f^*_n w^j_{k+n}\right) + 2qw^j_k - w^{j-1}_k, \\ d^{j+1}_k &= p\left(2w^j_k + \sum_{n=0}^{\infty} f_n d^j_{k-n} + \sum_{n=0}^{\infty} f^*_n d^j_{k+n}\right) + 2qd^j_k - d^{j-1}_k. \end{aligned} \tag{A.9}$$

In order to use (A.9), the coefficients for $j = 0$ and $j = 1$ have to be defined explicitly. Since

$$B_0(f(x)) \equiv 1\,, \quad B_0'(f(x)) \equiv 0\,,$$

$$B_1(f(x)) = p \cdot f(x) + q = pf_0 + q + \sum_{n=1}^{\infty} \frac{1}{2} pf_n \exp(in\alpha x) + \sum_{n=1}^{\infty} \frac{1}{2} pf^*_n \exp(-in\alpha x),$$

$$DB_1(f(x)) \equiv p\,,$$

one obtains the following starting formulas:

$$\begin{aligned} &w^0_0 = 1\,, \quad w^0_k = 0 \quad \text{for} \quad k > 0\,, \\ &w^1_0 = pf_0 + q\,, \quad w^1_k = \frac{1}{2} pf_k \quad \text{for} \quad k > 0\,, \\ &d^0_k = 0 \quad \text{for} \quad k \geq 0\,, \\ &d^1_0 = p\,, \quad d^1_k = 0 \quad \text{for} \quad k > 0\,. \end{aligned} \tag{A.10}$$

Appendix B. The operators in the stability equations (3.9)

The differential operators appearing in the stability equations (3.9) are defined as follows

$$G_v^{m,n} = \mathrm{Re}\cdot\left[\frac{i\,n\alpha}{k_{m-n}^2}\left(\beta^2 - t_m t_{m-n}\right) DF_u^n\, D + \frac{k_m^2}{k_{m-n}^2}\left(\beta^2 + t_{m-n}t_{m-2n}\right) F_v^n\, D\right.$$
$$+ \frac{i}{k_{m-n}^2}\left(2n\alpha\beta^2 - t_m k_{m-n}^2\right) F_u^n\, D^2 + \frac{i}{k_{m-n}^2}\left(n\alpha t_m - k_m^2\right) F_v^n\, D^3$$
$$\left. + i\,k_m^2 t_{m-2n} F_u^n + i\,t_m D^2 F_u^n\right],$$

$$\overline{G}_v^{m,n} = \mathrm{Re}\cdot\left[\frac{i\,n}{\alpha} k_{m+n}^2\left(t_m t_{m+n} - \beta^2\right)\left(DF_u^n\right)^*\, D\right.$$
$$+ \frac{k_m^2}{k_{m+n}^2}\left(\beta^2 + t_{m+n}t_{m+2n}\right)\left(F_v^n\right)^*\, D + \frac{i}{k_{m+n}^2}\left(-2n\alpha\beta^2 - t_m k_{m+n}^2\right)\left(F_u^n\right)^* D^2$$
$$\left. + \frac{i}{k_{m+n}^2}\left(-n\alpha t_m - k_m^2\right)\left(F_v^n\right)^*\, D^3 + i\,k_m^2 t_{m+2n}\left(F_u^n\right)^* + i\,t_m\left(D^2 F_u^n\right)^*\right],$$

$$G_\theta^{m,n} = \mathrm{Re}\cdot\left[\frac{1}{k_{m-n}^2} 2n\alpha\,\beta t_{m-n} F_u^n\, D + \frac{n\alpha\beta}{k_{m-n}^2}\left(t_m + t_{m-n}\right) DF_u^n\right.$$
$$\left. - \frac{i\,n\alpha\beta k_m^2}{k_{m-n}^2} F_v^n - \frac{i\,n\alpha\beta}{k_{m-n}^2} F_v^n\, D^2\right],$$

$$\overline{G}_\theta^{m,n} = \mathrm{Re}\cdot\left[-\frac{1}{k_{m+n}^2} 2n\alpha\,\beta t_{m+n}\left(F_u^n\right)^*\, D - \frac{n\alpha\beta}{k_{m+n}^2}\left(t_m + t_{m+n}\right)\left(DF_u^n\right)^* +\right.$$
$$\left. + \frac{i\,n\alpha\beta k_m^2}{k_{m+n}^2}\left(F_v^n\right)^* + \frac{i\,n\alpha\beta}{k_{m+n}^2}\left(F_v^n\right)^*\, D^2\right],$$

$$E_v^{m,n} = \mathrm{Re}\cdot\left[\beta DF_u^n - \frac{i\,n\alpha\beta}{k_{m-n}^2} F_v^n\, D^2\right],$$

$$\overline{E}_v^{m,n} = \mathrm{Re}\cdot\left[\beta\left(DF_u^n\right)^* + \frac{i\,n\alpha\beta}{k_{m+n}^2}\left(F_v^n\right)^* D^2\right],$$

$$E_\theta^{m,n} = \mathrm{Re}\cdot\left[-i\,t_m F_u^m - \frac{1}{k_{m-n}^2}\left(\beta^2 + t_m t_{m-n}\right) F_v^n\, D\right],$$

$$\overline{E}_\theta^{m,n} = \mathrm{Re}\cdot\left[-i\,t_m\left(F_u^m\right)^* - \frac{1}{k_{m+n}^2}\left(\beta^2 + t_m t_{m+n}\right)\left(F_v^n\right)^* D\right].$$

Appendix C. Inverse iterations method

In this work, the following form of IIM has been used:

START : λ_0 – inititial approximation of an eigenvalue,

$\mathbf{z}_0$ – inititial approximation of an eigenvector. $\|\mathbf{z}_0\| = 1$

$p_0 = 0$

REPEAT for k = 0, 1, .. :

1) Solve $(\mathbf{A} - \lambda_0 \mathbf{B})\, \mathbf{w}_{k+1} = \mathbf{B}\mathbf{z}_k$

2) Compute $p_{k+1} = \langle \mathbf{w}_{k+1}, \mathbf{z}_k \rangle^{-1}$

3) If $|p_{k+1} - p_k| > \varepsilon$ then

normalize $\mathbf{z}_{k+1} = \mathbf{w}_{k+1} / \|\mathbf{w}_{k+1}\|_2$

go to step 1

Else

compute the eigenvalue $\lambda = \lambda_0 + p_{k+1}$

compute the normalized eigenvector $\mathbf{z} = \mathbf{w}_{k+1} / \|\mathbf{w}_{k+1}\|_2$

STOP

End If

END.

References

1. J. M. FLORYAN, *Stability of wall-bounded shear layers in the presence of simulated distributed surface roughness,* Journal of Fluid Mechanics, **335**, 29-55, 1997.
2. A. CABAL, *Stability of wall-bounded flow modified due to the presence of distributed surface roughness,* Ph.D. thesis, The University of Western Ontario, London, Ontario, Canada, 1998.
3. A. CABAL, J. SZUMBARSKI, J. M. FLORYAN, *Stability of flow in a wavy channel,* Journal of Fluid Mechanics, **457**, pp. 191-212, 2002.
4. J. SZUMBARSKI, J. M. FLORYAN, *A direct spectral method for determination of flows over corrugated boundaries,* Journal of Computational Physics **153,** 378-402, 1999.
5. C. CANUTO, M. Y. HUSSAINI, A. QUARTERONI, T. A. ZANG, *Spectral Methods in Fluid Dynamics,* Springer Verlag, Berlin/New York, 1988.
6. J. SZUMBARSKI, *On origin of unstable modes in viscous channel flow subject to periodically distributed surface suction,* Preprint, Warsaw University of Technology, Warsaw, Poland. To appear in Theoretical and Applied Mechanics 4/2002.

7. J. M.FLORYAN, U. DALLMANN, *Flow over a leading edge with distributed roughness,* Journal of Fluid Mechanics, **216,** 629-656, 1990.

8. A. CABAL, J. SZUMBARSKI, J. M. FLORYAN, *Numerical Simulation of Flows Over Corrugated Walls,* Computers & Fluids, **30** (6), 753-776, 2002.

Received January 31, revised version April 26, 2002.

Arch. Mech., **54**, 3, pp. 223–244, Warszawa 2002

The plane single crystal under off-axis uniaxial tension

A. CHENAOUI[(1)], F. SIDOROFF[(2)], M. DARRIEULAT[(3)], A. HIHI[(4)]

[(1)] *L.M.M.H., Faculté des Sciences et Techniques de Tanger, B.P. 416, Tanger, Morocco*

[(2)] *LTDS, UMR, C.N.R.S. 5513, Ecole Centrale de Lyon, B. P. 163, 69131 Ecully Cedex, France*

[(3)] *SMS, M.M.F., U.R.A., C.N.R.S. 1884, Ecole Nationale Supérieure des Mines de Saint Etienne, 158 cours Fauriel, 42023 Saint Etienne Cedex 2, France*

[(4)] *L.M.M., Faculté des Sciences de Rabat, B. P. 1014, Rabat Agdal, Morocco*

THE TENSILE BEHAVIOUR of a rigid-plastic single crystal obeying Schmid's law with isotropic hardening is investigated for an off-axis tensile test in one of its symmetry planes (plane single crystal). Identification of the active slip systems allows the determination of the plastic spin and the resulting evolution of the crystallographic directions. This results in the description of the tensile behaviour-stress and strain response, onset of instability – depending upon the initial orientation of the crystal and the hardening law.

Key words: anisotropic material; crystal plasticity; finite strain; microstructure.

Notations

$\mathbf{F}$	deformation gradient tensor
$\mathbf{P}$	plastic transformation tensor
$\mathbf{R}$	lattice rotation tensor
$\mathbf{L}$	velocity gradient tensor
$\mathbf{D}$	strain-rate tensor
$\mathbf{W}$	rotation rate-tensor
$\bar{\mathbf{D}}$	strain-rate tensor rotated in the crystallographic configuration
$\bar{\mathbf{W}}$	rotation rate-tensor rotated in the crystallographic configuration
$\mathbf{T}$	Cauchy stress tensor
$\bar{\mathbf{T}}$	Cauchy stress tensor rotated in the crystallographic configuration
$\overline{\mathbf{N}}^s$	the s^{th} "pseudo slip" system $\dot{\gamma}^s$ shear strain rate on the "pseudo slip" system(s)

τ^s resolved shear stress on the "pseudo slip" system (s)
τ_c critical resolved shear stress
$\bar{\gamma}$ accumulated slip
τ_0 initial resolved shear stress H, A, n hardening material constants
x_1, x_2, x_3 space coordinates in the laboratory frame
$\bar{x}_1, \bar{x}_2, \bar{x}_3$ space coordinates in the crystallographic frame
θ orientation of the tensile axis
σ tensile stress
ε tensile strain
η transverse strain
ζ shear strain
σ^I stress at the onset of necking
ε^I strain at the onset of necking

1. Introduction

ANISOTROPIC PLASTICITY at large strain is an important problem for many engineering applications and in particular, for deep drawing and metal forming. The anisotropy of the behaviour and its evolution as well as plastic instability are some important features to be described and it is now well understood that the plastic spin is an essential issue to be dealt with.

From a macroscopic point of view, the plastic spin can be either a priori defined from the deformation (kinematic rotating frame [1]) or a posteriori postulated from the evolution equation (plastic spin [2]). It has, for example, recently been shown in [3] that the plastic spin and the initial orientation play a very essential role for instability analysis in an orthotropic material with Hill's quadratic criterion and Loret's plastic spin equation [4].

From a microscopic point of view however, the plastic spin directly follows from the evolution of the crystallographic directions, which in turn results from crystallographic glide along the active systems of each grain. The mechanics of single crystal therefore should play an important part in understanding the plastic spin and its influence upon anisotropy evolution and plastic instability.

The purpose of the present work is to investigate this question in the special case of the off-axis tensile behaviour of a fcc single crystal in one of its symmetry planes (100) or (110). As shown in [5-7], the behaviour of the real 3D crystal can in this case be described through a two-dimensional model: the plane single crystal.

A rigid-plastic model with isotropic hardening will be used and attention will be focussed on the dependence of the tensile behaviour and of the necking limit according to Considère's criterion [8] upon the initial orientation of the crystal and the hardening law.

2. Mechanical framework

2.1. Plane single crystal

A single crystal is a three-dimensional anisotropic material. In general, a two dimensional strain state will result in a three dimensional stress and vice versa. This difficulty is usually skipped by considering some fictitious two-dimensional crystal (double slip model [9-11]).

However, if the 3D single crystal is considered in one of its symmetry plane, then plane stress and plane strain are compatible resulting in a true two-dimensional model: "The plane single crystal" which is defined by the kinematical equations:

$$\mathbf{F} = \mathbf{R}\,\mathbf{P}, \quad \dot{\mathbf{P}}\,\mathbf{P}^{-1} = \sum_{s}^{m} \dot{\gamma}^s \bar{\mathbf{N}}^s, \tag{2.1}$$

where $\mathbf{F}$, $\mathbf{P}$ and $\mathbf{R}$ respectively, denote the deformation gradient, the plastic transformation and the lattice rotation tensors, while $\bar{\mathbf{N}}^s$ is the plane pseudo-slip system, defined in the crystallographic (isoclinic) configuration, which represents the symmetric contribution of two symmetric systems to $\dot{\mathbf{P}}\,\mathbf{P}^{-1}$ ([5-6] and [12]).

The velocity gradient $\mathbf{L}$, strain rate $\mathbf{D} = (\mathbf{L})^S$ and rotation rate $\mathbf{W} = (\mathbf{L})^A$ then result as

$$\mathbf{L} = \dot{\mathbf{F}}\,\mathbf{F}^{-1} = \dot{\mathbf{R}}\,\mathbf{R}^T + \mathbf{R}\,\dot{\mathbf{P}}\,\mathbf{P}^{-1}\,\mathbf{R}^T, \tag{2.2}$$

$$\bar{\mathbf{D}} = \mathbf{R}^T\,\mathbf{D}\,\mathbf{R} = \sum_{s}^{m} \dot{\gamma}^s \left(\bar{\mathbf{N}}^s\right)^S, \tag{2.3}$$

$$\bar{\mathbf{W}} = \mathbf{R}^T\,\mathbf{W}\,\mathbf{R} = \mathbf{R}^T\dot{\mathbf{R}} + \sum_{s}^{m} \dot{\gamma}^s \left(\bar{\mathbf{N}}^s\right)^A, \tag{2.4}$$

where suffices $(\,)^S$ and $(\,)^A$ respectively, denote the symmetric and skew-symmetric part of any tensor, and where a superimposed bar denotes tensors rotated in the crystallographic configuration.

In the following, attention will be focussed on rate-independent plasticity (Schmid's law)

$$\dot{\gamma}^s \geq 0 \quad \text{if} \quad \tau^s = \tau_c\,, \quad \dot{\gamma}^s = 0 \quad \text{if} \quad |\tau^s| < \tau_c, \quad \dot{\gamma}^s \leq 0 \quad \text{if} \quad \tau^s = -\tau_c, \tag{2.5}$$

where τ_c is the critical resolved shear stress, and τ^s is the resolved shear stress defined as

$$\tau^s = \bar{\mathbf{T}}_{ij}\,\bar{\mathbf{N}}^s_{ij}, \quad \bar{\mathbf{T}} = \mathbf{R}^T\mathbf{T}\mathbf{R}, \tag{2.6}$$

with $\mathbf{T}$ being the usual Cauchy stress tensor as observed in the laboratory frame and $\bar{\mathbf{T}}$ the corresponding tensor in the crystallographic configuration.

In this work the uniform isotropic hardening will be assumed with the same τ_c for all systems. The hardening rule is taken as

$$\tau_c = \tau_c(\bar{\gamma}), \tag{2.7}$$

where

$$\dot{\bar{\gamma}} = \sum_s^m |\dot{\gamma}^s| \quad \text{and} \quad \bar{\gamma} = \int_0^T \dot{\bar{\gamma}} dt.$$

Two cases will be considered in the following:
- linear hardening

$$\tau_c = \tau_0(\,1 + \,H\,\bar{\gamma}\,), \tag{2.8}$$

- nonlinear power law hardening

$$\tau_c = \tau_0(\,1 + \,A\,(\bar{\gamma})^n\,), \tag{2.9}$$

where τ_0 is the initial resolved shear and H, A and n are material constants.

In this plane case, the rotation $\mathbf{R}$ and the stress tensor $\mathbf{T}$ are respectively given by

$$R = \begin{bmatrix} \cos(\theta) & \sin(\theta) & 0 \\ -\sin(\theta) & \cos(\theta) & 0 \\ 0 & 0 & 1 \end{bmatrix},$$

$$R^T \dot{R} = \dot{\theta} \begin{bmatrix} 0 & 1 & 0 \\ -1 & 0 & 0 \\ 0 & 0 & 0 \end{bmatrix}, \tag{2.10}$$

$$T = \begin{bmatrix} \sigma_1 & \tau & 0 \\ \tau & \sigma_2 & 0 \\ 0 & 0 & 0 \end{bmatrix},$$

with the following relations:

$$\begin{aligned} \bar{T}_{11} &= \frac{\sigma_1 + \sigma_2}{2} + \frac{\sigma_1 - \sigma_2}{2}\cos(2\theta) - \tau\sin(2\theta), \\ \bar{T}_{22} &= \frac{\sigma_1 + \sigma_2}{2} - \frac{\sigma_1 - \sigma_2}{2}\cos(2\theta) + \tau\sin(2\theta), \\ \bar{T}_{12} &= \frac{\sigma_1 - \sigma_2}{2}\sin(2\theta) + \tau\cos(2\theta). \end{aligned} \tag{2.11}$$

For a fcc single crystal there are 12 systems associated to the planes {111} and directions <110>. This 3D single crystal gives rise to two plane single crystals corresponding to a plane stress and strain state in the {100} and {110} planes, respectively. We shall therefore restrict our attention to these two cases, respectively denoted by Pfcc1 and Pfcc2 (plane fcc) single crystals. The crystallographic frame $(\bar{x}_1, \bar{x}_2, \bar{x}_3)$ is chosen

for Pfcc1 : $\bar{x}_1 = [100]$, $\bar{x}_2 = [010]$, $\bar{x}_3 = [001]$,

for Pfcc2 : $\bar{x}_1 = [001]$, $\bar{x}_2 = [1\bar{1}0]$, $\bar{x}_3 = [110]$.

The corresponding pseudo-slip systems are summarized in Table 1 (Pfcc 2 model) and Table 2 (Pfcc1 model) and the Reader is referred to Refs. [5-7] for further details.

It should be noted that the Pfcc2 single crystal presented here has recently been used by [13-15] for the bicrystal investigation in (110) channel die compression.

Table 1. Pfcc2 single crystal

System (s)	Resolved shear τ^s	Pseudo-slip $\overline{\mathbf{N}}^s$
1	$\tau^1 = \dfrac{\overline{\mathbf{T}}_{12}}{\sqrt{3}}$	$\overline{\mathbf{N}}^1 = \dfrac{1}{2\sqrt{3}} \begin{bmatrix} 0 & 0 \\ 2 & 0 \end{bmatrix}$
2	$\tau^2 = \dfrac{\overline{\mathbf{T}}_{12} - \sqrt{2}\,\overline{\mathbf{T}}_{11}}{2\sqrt{3}}$	$\overline{\mathbf{N}}^2 = \dfrac{1}{2\sqrt{3}} \begin{bmatrix} -\sqrt{2} & 0 \\ 1 & 0 \end{bmatrix}$
3	$\tau^3 = \dfrac{\overline{\mathbf{T}}_{12} + \sqrt{2}\,\overline{\mathbf{T}}_{11}}{2\sqrt{3}}$	$\overline{\mathbf{N}}^3 = \dfrac{1}{2\sqrt{3}} \begin{bmatrix} \sqrt{2} & 0 \\ 1 & 0 \end{bmatrix}$
4	$\tau^4 = \dfrac{\overline{\mathbf{T}}_{12} + \sqrt{2}\,(\overline{\mathbf{T}}_{11} - \overline{\mathbf{T}}_{22})}{2\sqrt{3}}$	$\overline{\mathbf{N}}^4 = \dfrac{1}{2\sqrt{3}} \begin{bmatrix} \sqrt{2} & 2 \\ -1 & -\sqrt{2} \end{bmatrix}$
5	$\tau^5 = \dfrac{\overline{\mathbf{T}}_{12} - \sqrt{2}\,(\overline{\mathbf{T}}_{11} - \overline{\mathbf{T}}_{22})}{2\sqrt{3}}$	$\overline{\mathbf{N}}^5 = \dfrac{1}{2\sqrt{3}} \begin{bmatrix} -\sqrt{2} & 2 \\ -1 & \sqrt{2} \end{bmatrix}$

2.2. Off-axis tensile test

Our attention is focussed here on off-axis tensile test [16], where the Cauchy stress $\mathbf{T}$ and the deformation gradient $\mathbf{F}$ are given, in the laboratory frame (x_1, x_2, x_3), by

$$\mathbf{T} = \begin{bmatrix} \sigma & 0 & 0 \\ 0 & 0 & 0 \\ 0 & 0 & 0 \end{bmatrix}, \quad \mathbf{F} = \begin{bmatrix} e^{\varepsilon} & \zeta\, e^{\varepsilon} & 0 \\ 0 & e^{\eta} & 0 \\ 0 & 0 & e^{-(\varepsilon+\eta)} \end{bmatrix}. \tag{2.12}$$

Table 2. Pfcc1 single crystal

System (s)	Resolved shear τ^s	Pseudo-slip $\overline{\mathbf{N}}^s$
1	$\tau^1 = \dfrac{\overline{\mathbf{T}}_{11} - \overline{\mathbf{T}}_{22}}{\sqrt{6}}$	$\overline{\mathbf{N}}^1 = \dfrac{1}{\sqrt{6}}\begin{bmatrix} 1 & 1 \\ -1 & -1 \end{bmatrix}$
2	$\tau^2 = \dfrac{\overline{\mathbf{T}}_{11} + \overline{\mathbf{T}}_{12}}{\sqrt{6}}$	$\overline{\mathbf{N}}^2 = \dfrac{1}{\sqrt{6}}\begin{bmatrix} 1 & 1 \\ 0 & 0 \end{bmatrix}$
3	$\tau^3 = \dfrac{\overline{\mathbf{T}}_{22} + \overline{\mathbf{T}}_{12}}{\sqrt{6}}$	$\overline{\mathbf{N}}^3 = \dfrac{1}{\sqrt{6}}\begin{bmatrix} 0 & 0 \\ 1 & 1 \end{bmatrix}$
4	$\tau^4 = \dfrac{\overline{\mathbf{T}}_{11} - \overline{\mathbf{T}}_{12}}{\sqrt{6}}$	$\overline{\mathbf{N}}^4 = \dfrac{1}{\sqrt{6}}\begin{bmatrix} 1 & -1 \\ 0 & 0 \end{bmatrix}$
5	$\tau^5 = \dfrac{\overline{\mathbf{T}}_{12} - \overline{\mathbf{T}}_{22}}{\sqrt{6}}$	$\overline{\mathbf{N}}^5 = \dfrac{1}{\sqrt{6}}\begin{bmatrix} 0 & 0 \\ 1 & -1 \end{bmatrix}$
6	$\tau^6 = \dfrac{\overline{\mathbf{T}}_{11} - \overline{\mathbf{T}}_{22}}{\sqrt{6}}$	$\overline{\mathbf{N}}^6 = \dfrac{1}{\sqrt{6}}\begin{bmatrix} 1 & -1 \\ 1 & -1 \end{bmatrix}$

The strain components ε, η and ζ are given by

$$\frac{h}{h_0} = e^{\varepsilon}, \quad \frac{d}{d_0} = e^{\eta}, \quad \zeta = e^{-(\varepsilon+\eta)}\,\mathrm{tg}(\xi),$$

where (h_0, d_0) and (h, d) respectively, denote the initial and the current length and width of specimen, and where ξ is the rotation of the final section (Fig. 1).

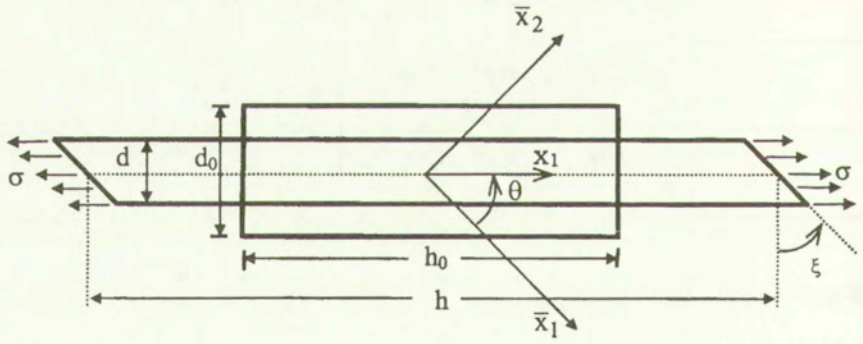

FIG. 1. Off-axis uniaxial tensile test.

The tensile direction x_1 is taken in the crystallographic plane $(\bar{x}_1, \bar{x}_2)$ previously defined.

The lattice angle θ is the angle between the x_1 tensile direction and the fixed lattice orientation $\bar{x}_1$. The strain rate $\mathbf{D}$ and rotation rate $\mathbf{W}$ are obtained from

Eq. (2.12) as

$$D_{11} = \dot{\varepsilon} \ , \ D_{22} = \dot{\eta} \ , \ D_{12} = W_{12} = \frac{\dot{\zeta}}{2} e^{\varepsilon - \eta}, \tag{2.13}$$

or in terms of the rotated tensor $\bar{\mathbf{D}}$ introduced in Eq. (2.3)

$$\begin{aligned} \dot{\varepsilon} &= \frac{\bar{D}_{11} + \bar{D}_{22}}{2} + \frac{\bar{D}_{11} - \bar{D}_{22}}{2} \cos(2\theta) + \bar{D}_{12} \sin(2\theta), \\ \dot{\eta} &= \frac{\bar{D}_{11} + \bar{D}_{22}}{2} - \frac{\bar{D}_{11} - \bar{D}_{22}}{2} \cos(2\theta) - \bar{D}_{12} \sin(2\theta), \\ \dot{\zeta} &= 2e^{(\eta - \varepsilon)} \left\{ -\frac{\bar{D}_{11} - \bar{D}_{22}}{2} \sin(2\theta) + \bar{D}_{12} \cos(2\theta) \right\}, \end{aligned} \tag{2.14}$$

where $\bar{D}_{ij}$ are given from $\dot{\gamma}^s$ by Eq. (2.3) and Table 1 (resp. table 2) for Pfcc2 (resp. Pfcc1) single crystal.

Similarly, by combining Eqs. (2.4), (2.6), (2.10) and (2.13), the lattice spin equation and the rotated stress tensor $\bar{\mathbf{T}}$ can be expressed as

$$W_{12} = \dot{\theta} + \frac{1}{2} \sum_{s}^{m} \dot{\gamma}^s \left\{ \bar{N}^s_{12} - \bar{N}^s_{21} \right\}, \tag{2.15}$$

$$\bar{T}_{11} = \frac{\sigma}{2}(1 + \cos(2\theta)), \quad \bar{T}_{22} = \frac{\sigma}{2}(1 - \cos(2\theta)), \quad \bar{T}_{12} = \frac{\sigma}{2} \sin(2\theta). \tag{2.16}$$

3. The Pfcc 2 single crystal

3.1. System activity

According to Eq. (2.16) and Table 1, the resolved shear stresses τ^s are given by

$$\tau^s = f^s(\theta) \ \sigma, \tag{3.1}$$

where the functions $f^s(\theta)$ are respectively defined by

$$\begin{aligned} f^1(\theta) &= \frac{1}{2\sqrt{3}} \left\{ \sin(2\theta) \right\}, \\ f^2(\theta) &= \frac{1}{4\sqrt{3}} \left\{ -\sqrt{2} + \sin(2\theta) - \sqrt{2} \cos(2\theta) \right\}, \\ f^3(\theta) &= \frac{1}{4\sqrt{3}} \left\{ \sqrt{2} + \sin(2\theta) + \sqrt{2} \cos(2\theta) \right\}, \\ f^4(\theta) &= \frac{1}{4\sqrt{3}} \left\{ \sin(2\theta) + 2\sqrt{2} \cos(2\theta) \right\}, \\ f^5(\theta) &= \frac{1}{4\sqrt{3}} \left\{ \sin(2\theta) - 2\sqrt{2} \cos(2\theta) \right\}. \end{aligned} \tag{3.2}$$

For a given θ, there will usually be one active system corresponding to the maximum absolute value of the five quantities f^s defined in relation (3.2). The corresponding system activity is described as a function of θ in Table 3 with $\mathrm{tg}(2\theta_p) = 2\sqrt{2}$. The tensile stress now follows as a function of θ by

$$\sigma = \frac{\tau_c}{|\, f^s(\theta)\,|}. \tag{3.3}$$

Table 3. System activity for the Pfcc2 single crystal

θ	Active system	Activity conditions	Slip rates
0			
	3^+	$\tau^3 = \tau_c$ and $\dot{\tau}^3 = \dot{\tau}_c$	$\dot{\gamma}^3 \geq 0$
$\pi/2 - \theta_p$			
	5^+	$\tau^5 = \tau_c$ and $\dot{\tau}^5 = \dot{\tau}_c$	$\dot{\gamma}^5 \geq 0$
$\pi/2$			
	4^-	$\tau^4 = -\tau_c$ and $\dot{\tau}^4 = -\dot{\tau}_c$	$\dot{\gamma}^4 \leq 0$
$\pi/2 + \theta_p$			
	2^-	$\tau^2 = -\tau_c$ and $\dot{\tau}^2 = -\dot{\tau}_c$	$\dot{\gamma}^2 \leq 0$
π			

The corresponding curve $\dfrac{\sigma}{\tau_c}$ is represented in Fig. 2.

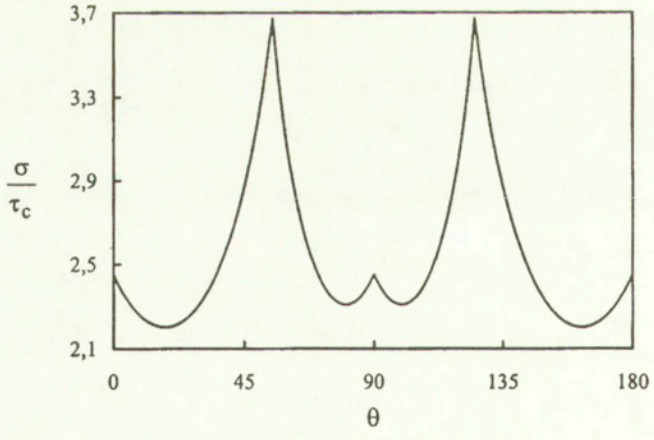

FIG. 2. The Pfcc 2 versus $\dfrac{d\theta}{d\varepsilon}$ versus the crystal orientation θ.

3.2. Lattice rotation

Once the active system is known, the kinematical analysis directly proceeds from the relations (2.3) and (2.15). Since the system (1) is never active, these equations are reduced to

$$\bar{D}_{11} = \frac{1}{\sqrt{6}} \{ \dot{\gamma}^3 + \dot{\gamma}^4 - \dot{\gamma}^5 - \dot{\gamma}^2 \},$$

$$\bar{D}_{22} = \frac{1}{\sqrt{6}} \{ \dot{\gamma}^5 - \dot{\gamma}^4 \}, \tag{3.4}$$

$$\bar{D}_{12} = \frac{1}{4\sqrt{3}} \{ \dot{\gamma}^2 + \dot{\gamma}^3 + \dot{\gamma}^4 + \dot{\gamma}^5 \},$$

$$W_{12} = \dot{\theta} - \frac{1}{4\sqrt{3}} \{ 3\dot{\gamma}^4 + 3\dot{\gamma}^5 - \dot{\gamma}^2 - \dot{\gamma}^3 \}. \tag{3.5}$$

For instance, if the active system is the system (3), the Eq. (3.4) becomes

$$\bar{D}_{11} = \frac{1}{\sqrt{6}} \dot{\gamma}^3, \quad \bar{D}_{22} = 0, \quad \bar{D}_{12} = \frac{1}{4\sqrt{3}} \dot{\gamma}^3, \tag{3.6}$$

which give from Eq. (2.14)

$$\dot{\gamma}^3 = \frac{\dot{\varepsilon}}{f^3(\theta)}, \tag{3.7}$$

with the same function $f^3(\theta)$ as in Eq. $(3.2)_3$.

Using Eqs. (2.13), (2.14), (3.5) and (3.6), the component W_{12} can be written as

$$W_{12} = \frac{\dot{\zeta}}{2} e^{(\varepsilon - \eta)} = \frac{\cos(2\theta) - \sqrt{2}\sin(2\theta)}{4\sqrt{3}\, f^3(\theta)} \dot{\varepsilon}. \tag{3.8}$$

Combining Eqs. (3.7) and (3.8), the evolution Eq. (3.5) gives $\frac{\dot{\theta}}{\dot{\varepsilon}} = \frac{d\theta}{d\varepsilon}$ as

$$\frac{d\theta}{d\varepsilon} = \frac{g^3(\theta)}{f^3(\theta)}, \tag{3.9}$$

where

$$g^3(\theta) = \frac{1}{4\sqrt{3}} \left\{ 1 - \sqrt{2}\sin(2\theta) + \cos(2\theta) \right\}. \tag{3.10}$$

The other cases are analyzed in a similar way. More generally, we obtain for each active system (s)

$$\dot{\gamma}^s = \frac{\dot{\varepsilon}}{f^s(\theta)}, \tag{3.11}$$

$$\frac{d\theta}{d\varepsilon} = \frac{g^s(\theta)}{f^s(\theta)}, \tag{3.12}$$

where the functions $f^s(\theta)$ are defined in Eqs. (3.2) and $g^s(\theta)$ are respectively, defined by

$$\begin{aligned}
g^2(\theta) &= \frac{1}{4\sqrt{3}}\left\{1+\sqrt{2}\sin(2\theta)+\cos(2\theta)\right\}, && 0 \le \theta \le \frac{\pi}{2}-\theta_p,\\
g^3(\theta) &= \frac{1}{4\sqrt{3}}\left\{1-\sqrt{2}\sin(2\theta)+\cos(2\theta)\right\}, && \frac{\pi}{2}-\theta_p \le \theta \le \frac{\pi}{2},\\
g^4(\theta) &= \frac{1}{4\sqrt{3}}\left\{-3-2\sqrt{2}\sin(2\theta)+\cos(2\theta)\right\}, && \frac{\pi}{2} \le \theta \le \frac{\pi}{2}+\theta_p,\\
g^5(\theta) &= \frac{1}{4\sqrt{3}}\left\{2\sqrt{2}\sin(2\theta)+\cos(2\theta)-3\right\}, && \frac{\pi}{2}+\theta_p \le \theta \le \pi.
\end{aligned} \tag{3.13}$$

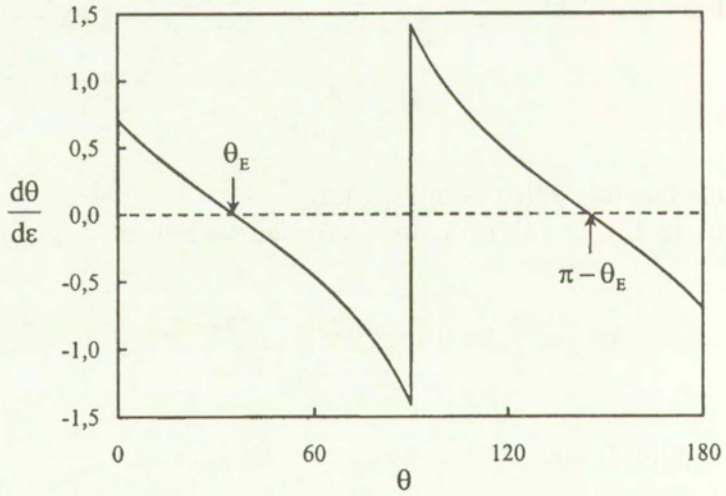

FIG. 3. The Pfcc 2 plastic spin $\frac{d\theta}{d\varepsilon}$ versus the crystal orientation θ.

The function $\frac{d\theta}{d\varepsilon}$ is represented in Fig. 3. The lattice rotation evolution, from its initial value θ_0, directly follows from this curve. For instance, if $0 \le \theta_0$

$\leq \theta_E\left(\mathrm{tg}(\theta_E) = \dfrac{1}{\sqrt{2}}\right)$, $\dfrac{d\theta}{d\varepsilon}$ is positive so that θ increases and tends to the stable orientation θ_E, while if $\theta_E \leq \theta_0 \leq \pi/2$, θ decreases toward the same stable orientation. Similar results are obtained for $\pi/2 \leq \theta_0 \leq \pi$. This evolution is represented in Fig. 4.

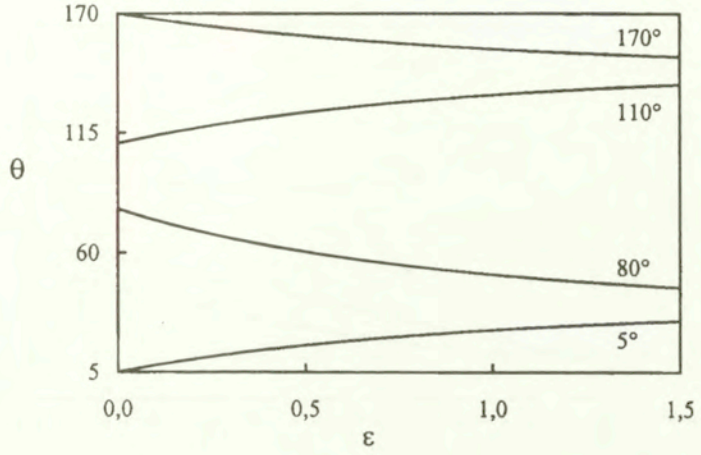

FIG. 4. The Pfcc 2 lattice spin versus the strain ε, for various values of initial orientation θ_0.

3.3. Stress and strain response

The stress response $\sigma(\varepsilon)$ directly follows as

$$\sigma(\varepsilon) = \frac{\tau_c(\bar{\gamma})}{|\, f^s(\theta)\,|}, \tag{3.14}$$

where θ and $\bar{\gamma}$ are obtained, as a function of ε, through the integration of the expression (3.11) and (3.12) of $\dfrac{d\gamma}{d\varepsilon}$ and $\dfrac{d\theta}{d\varepsilon}$.

This response is illustrated in Figs. 5a-b (linear hardening) and Figs. 6a-b (power law), for various values of θ_0. It can be seen that, depending on the crystal orientation and on the hardening rule, the tensile response σ may be an increasing or decreasing function of ε (a negative or a positive hardening). Negative hardening however will decrease when the mechanical hardening increases. This is illustrated in Fig. 7 which for linear hardening shows the angular region corresponding to tensile negative hardening as a function of the hardening parameter H. In particular, negative hardening disappears for $H \simeq 0.4$ which is a rather high value.

Similarly, for the strain, the corresponding differential system, which by integration gives η and ζ in terms of ε, is easily obtained from Eqs. (2.14), (3.4), (3.11) and (3.12).

The corresponding evolution, which in fact does not depend on the hardening, is plotted in Figs. 8a-b for different values of θ_0. These results illustrate clearly the effect of rotation on the single crystal behaviour.

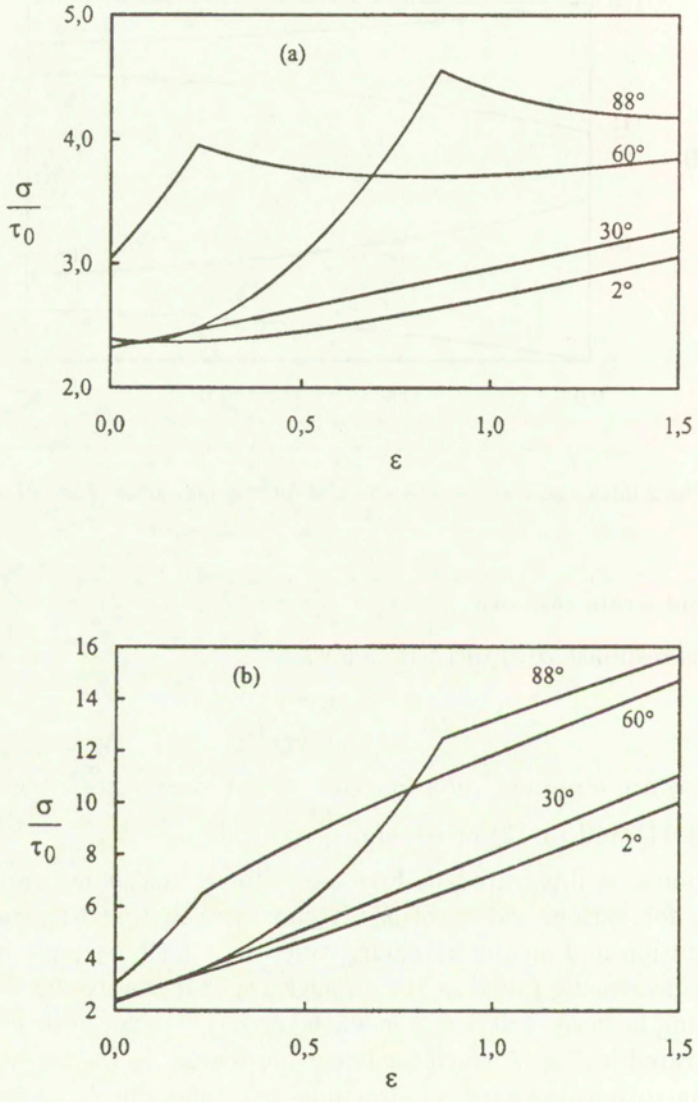

FIG. 5. The Pfcc 2 tensile response σ versus the strain ε, for various values of initial orientation θ_0 and with linear hardening. (a) when $H = 0.1$ (b) when $H = 1$.

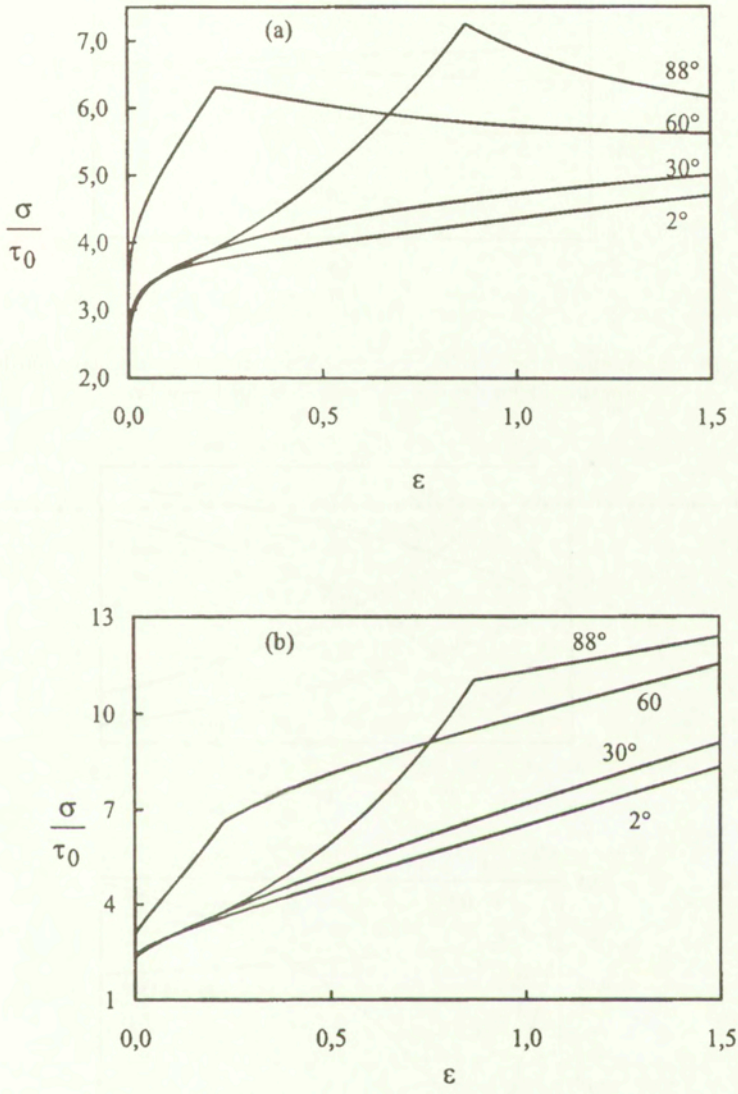

FIG. 6. The Pfcc 2 tensile response σ versus the strain ε, for various values of initial orientation θ_0 and with power law hardening. (a) when $A = 1$ and $n = 0.2$, (b) when $A = 1$ and $n = 0.8$

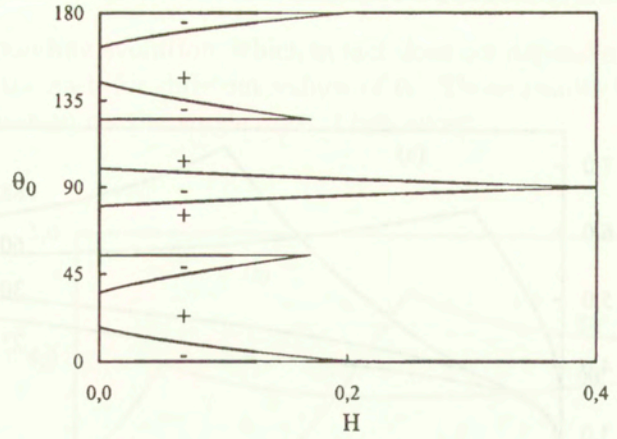

FIG. 7. The Pfcc 2 angular region (H, θ_0) corresponding to tensile negative hardening as a function of hardening parameter H for linear law.

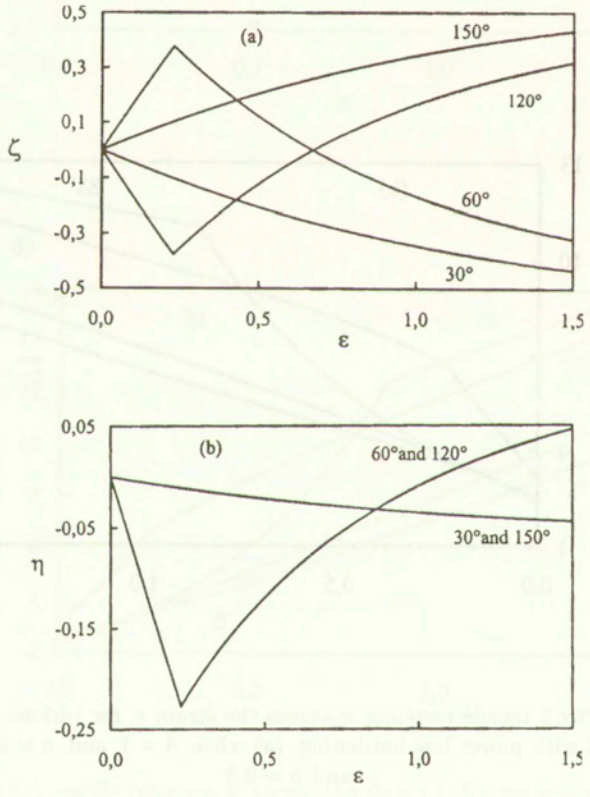

FIG. 8. The Pfcc 2 strain response for various values of initial orientation; (a) the shear ζ versus the strain ε, (b) the transverse strain η versus the strain ε.

4. Plastic instability

4.1. Considère's analysis

We are now interested in the necking instability which may occur during a tensile test. Considère's necking criterion is used [8], which associates necking to the maximum of the tensile force $P = S\sigma = S_0\sigma e^{-\varepsilon}$ (plastic incompressibility), leading to the following criterion:

$$\frac{1}{\sigma}\frac{d\sigma}{d\varepsilon} = 1. \tag{4.1}$$

In this relation σ is given by Eq. (3.14), while $\dfrac{d\sigma}{d\varepsilon}$ is calculated, for each active system (s), from the activation condition (2.5)

$$\dot{\sigma}^s = \operatorname{sgn}(f^s)\dot{\tau}_c, \tag{4.2}$$

where sgn(x) is the sign of the scalar quantity x.

Using Eq. (3.1), this gives

$$\sigma\frac{df^s}{d\theta}\frac{g^s}{f^s} + f^s\frac{d\sigma}{d\varepsilon} = \operatorname{sgn}(f^s)\frac{d\tau_c}{d\varepsilon},$$

providing $\dfrac{d\sigma}{d\varepsilon}$ as:

- for linear hardening (Eq. (2.8))

$$\frac{d\sigma}{d\varepsilon} = \frac{H\tau_0 - \Psi^s}{(f^s)^2}, \tag{4.3}$$

- for nonlinear hardening (Eq. (2.9))

$$\frac{d\sigma}{d\varepsilon} = \frac{nA\tau_0\ (\bar{\gamma})^{n-1} - \Psi^s}{(f^s)^2}, \tag{4.4}$$

where the function $\Psi^s(\theta, \sigma)$ is defined by

$$\Psi^s(\theta, \sigma) = g^s\frac{df^s}{d\theta}\sigma.$$

For a given tensile test the stress σ^I and strain ε^I, corresponding to the onset of necking, are then easily deduced from the criterion introduced in Eq. (4.1).

4.2. Applications

The values of σ^I and ε^I, as a function of the initial orientation θ_0 and for different cases of hardening, are represented in Figs. 9a-b and 10a-b.

This illustrates the combined effect of hardening and orientation on necking. It should be noted that in agreement with Fig. 7, necking can happen from the very beginning ($\varepsilon^I = 0$). The corresponding region in the (θ_0, H)-plane (for linear hardening) is represented in Fig. 11.

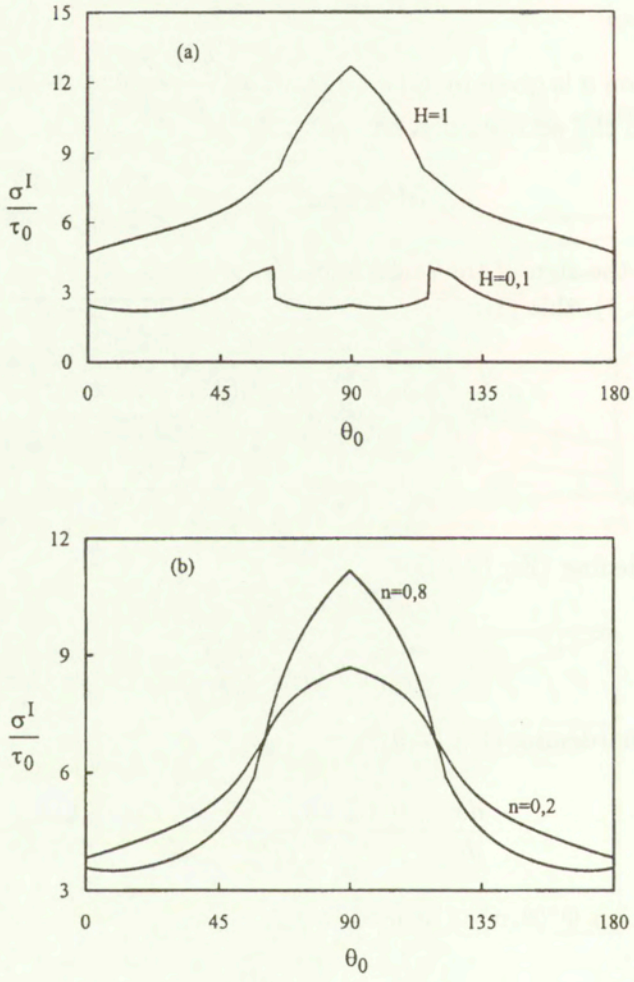

FIG. 9. The Pfcc 2 tensile stress σ^I at the onset of necking versus the initial orientation θ_0 (a) linear hardening, (b) power law hardening when $A = 1$.

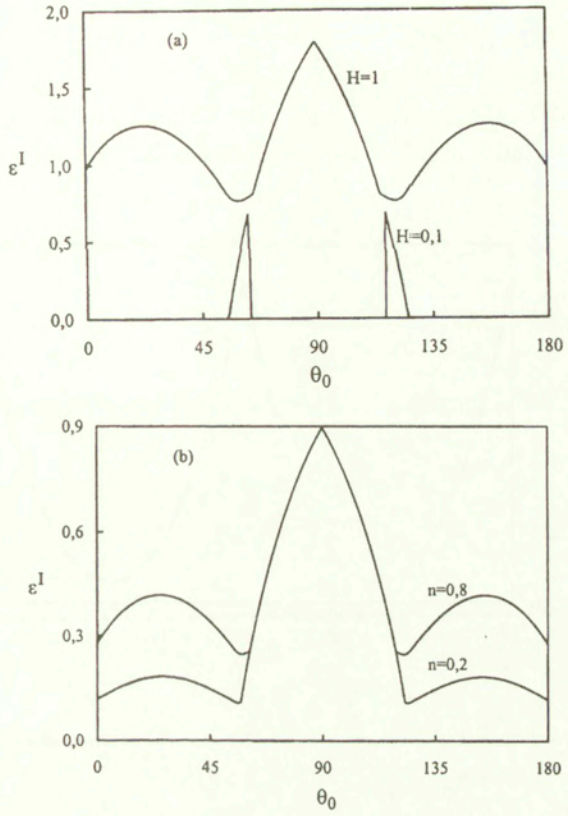

FIG. 10. The Pfcc 2 tensile strain ε^I at the onset of necking versus the initial orientation θ_0; (a) linear hardening, (b) power law hardening when $A = 1$.

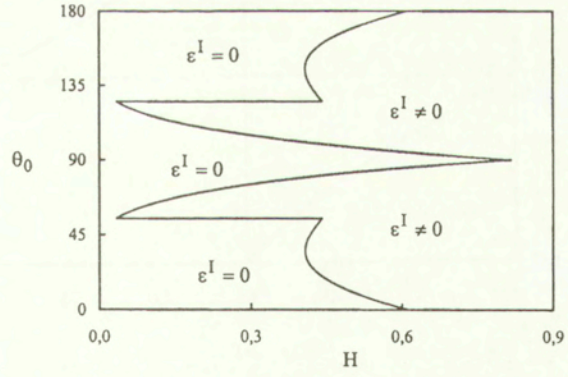

FIG. 11. The Pfcc 2 initial orientation as function of linear hardening parameter H corresponding to $\varepsilon^I = 0$.

5. The Pfcc 1 behaviour

Similar analysis can be performed in the Pfcc1 case and the corresponding results (Figs. 12-16 and Tabl. 4) are presented below without further details.

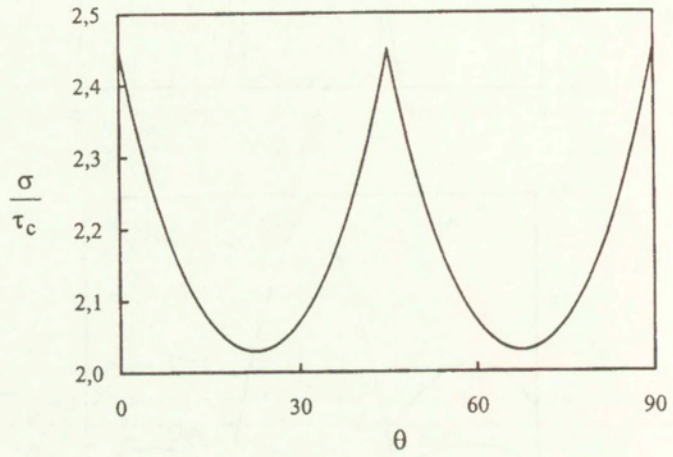

FIG. 12. The Pfcc 1 $\frac{\sigma}{\tau_c}$ versus the crystal orientation θ.

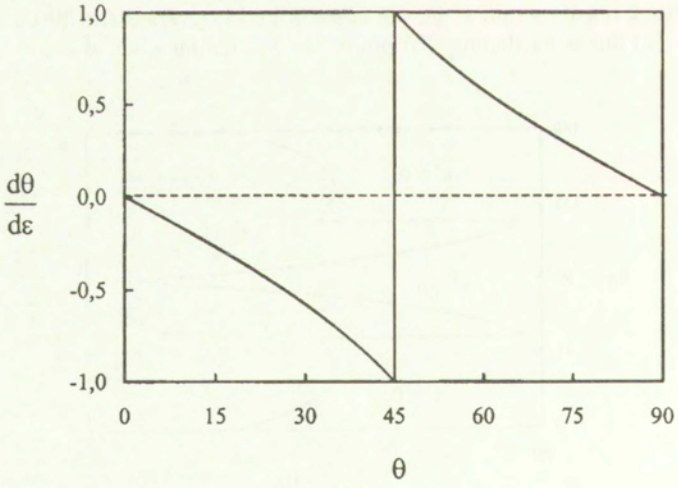

FIG. 13. The Pfcc 1 plastic spin $\frac{d\theta}{d\varepsilon}$ versus the crystal orientation θ.

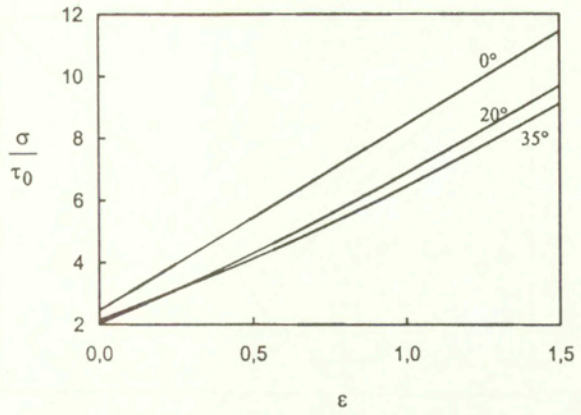

FIG. 14. The Pfcc 1 tensile response σ versus the strain ε, for various values of initial orientation θ_0. Linear hardening when $H = 1$.

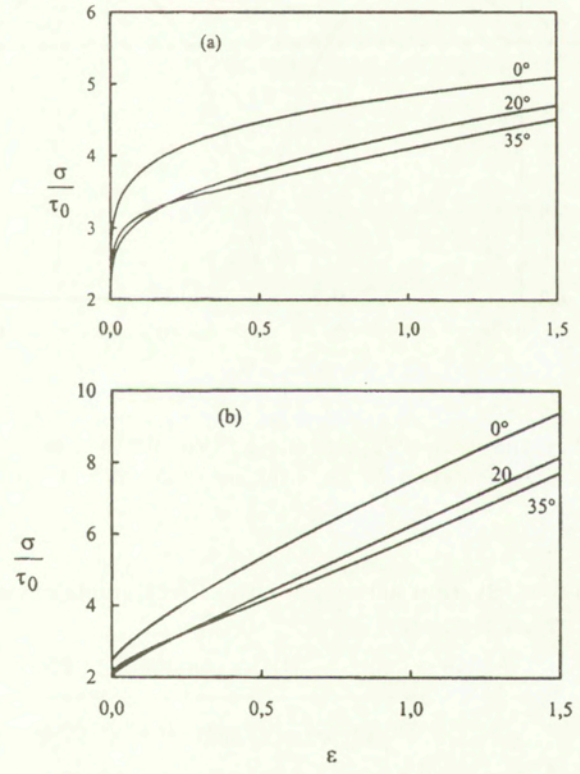

FIG. 15. The Pfcc 1 tensile response σ versus the strain ε, for various values of initial orientation θ_0. Power law hardening with $A = 1$: (a) when $n = 0.2$; (b) when $n = 0.8$.

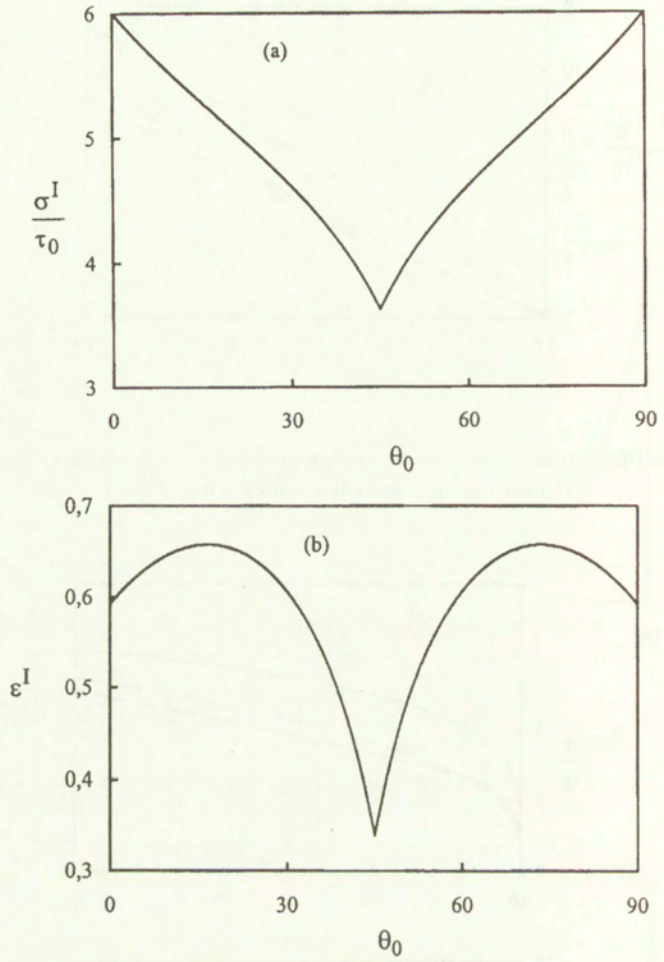

FIG. 16. The Pfcc 1 tensile stress $\sigma^I(a)$ and strain ε^I (b) at the onset of necking versus the initial orientation θ_0, for linear hardening with $H = 1$.

Table 4. System activity for the Pfcc1 single crystal

θ	Active system	Activity conditions	Slip rates
0			
	2^+	$\tau^2 = \tau_c$ and $\dot{\tau}^2 = \dot{\tau}_c$	$\dot{\alpha}^2 \geq 0$
$\pi/4$			
	3^+	$\tau^3 = \tau_c$ and $\dot{\tau}^3 = \dot{\tau}_c$	$\dot{\alpha}^3 \geq 0$
$\pi/2$			

6. Conclusions

A f.c.c. single crystal undergoing stress in one of its symmetry planes {110} or {100} retains this element of symmetry throughout the deformation. Taking advantage of the consequent simplifications, a fully analytical investigation of the plastic behaviour is possible in the case of large strain deformations.

In the present paper, the case of the off-axis uniaxial tension of a rigid plastic crystal is presented. Double slip is activated from the onset on symmetric slip systems, leading to a case of "plane deformation" that can actually be observed in real crystals. Strain hardening is taken as isotropic, but with various hypotheses. The rotation of the crystal with respect to the tensile axis is calculated, and stability is put in evidence when the tension is performed along the $< 1\bar{1}2 >$ direction (plane of symmetry {110}) or the $< 001 >$ direction (plane of symmetry {100}) . The possibility of softening is put in evidence for specific ranges of the initial orientation. The dependence of the threshold of strain localisation on a combination of crystal rotation and strain hardening effects is shown in the simple case of Considère's criterion.

This study completes previous investigations on the simple shear and the torsion in similar symmetry conditions, aiming at a full understanding of the two-dimensional behaviour of crystals.

Acknowledgements

This work was supported in part by the Morocco National Center of Coordination and Planning of Scientific and Technique Research (PARS Program SPI N ° 101) and one of the authors (A.C.) wants to express his gratitude to Region Rhone-Alpes for generous financial support of his stay at the Ecole des Mines de Saint Etienne.

References

1. A. DOGUI and F. SIDOROFF, *Rhéologie anisotrope en grandes déformations,* [in:] Proc. Conf. on Rhéologie des Materiaux Anisotropes C. HUET, D. BOURGON and S. RICHEMOND)[Eds.], CEPADUES, Toulouse, 69–78, 1986.
2. Y. F. DAFALIAS, *The spin plastic,* J. Appl. Mech., ASME **52**, 865–871, 1985.
3. H. LEE, IM S. and S. N. ATLURI, *Strain localization in an orthotropic material with plastic spin,* Int. J. of Plasticity, **11**, 4, 423–450, 1995.
4. B. LORET and Y. F. DAFALIAS, *The effect of anisotropy and plastic spin on fold deformations,* J. Mech. Phys. Solids, **40** 417, 1992.
5. J. BOUKADIA and F. SIDOROFF, *Simple shear and torsion of a perfectly plastic single crystal in finite transformation,* Arch. Mech. **40**, 497-513, 1988.

6. J. BOUKADIA, A. CHENAOUI and F. SIDOROFF, *Simple shear in fcc single crystals at large deformations,* in Proc. Int. Sem. MECAMAT'91 Faintainebleau /France/ on Large Plastic Deformation C. TEODOSIU, J. L. RAPHANEL and F. SIDOROFF. Rotterdam Balkema, 109-116, 1993.

7. A. CHENAOUI, F. SIDOROFF and A. HIHI, *The texture evolution of planar polycrystal,* J. Mech. Phys. Solids, **48**, 2559-2584, 2000.

8. A. CONSIDÈRE, *Mémoire sur l'emploi du fer et de l'acier dans les constructions*, Annales des Ponts et Chaussées, **9**, 574, 1858.

9. R. J. ASARO, *Geometrical effects in the inhomogeneous deformation of ductile single crystals,* Acta Metall. **27**, 445-453, 1979.

10. K S. HAVNER, *The kinematics of double slip with application to cubic crystals in the compression test,* J. Mech. Phys. Solids, **27**, 415-429, 1979.

11. A. H. SHALABY and K. S. HAVNER, *A general kinematical analysis of double slip,* J. Mech. Phys. Solids, **26**, 79-92, 1978.

12. A. CHENAOUI, *Contribution à l'étude du comportement du monocristal en grandes déformations plastique,* Thesis, Ecole Centrale de Lyon, N° 92-13, 1992.

13. K. S. HAVNER, S.-C. WU and S. FUH, *On symmetric bicrystals at the yield point in (110) channel die compression,* J. Mech. Phys. Solids, **42**, 361-379, 1994.

14. K. S. HAVNER, *On velocity discontinuities in elastoplastic bicrystals in channel die compression,* Int. J. of Plasticity, **14**, 61-74, 1998.

15. P. YU and K. S. HAVNER, *Numerical studies of nonuniform deformation, stress state evolution, and subgrain formation in bicrystals in (110) channel die compression,* J. Mech. Phys. Solids, **49**, 173-208, 2001.

16. A. DOGUI, Cinématique bidimensionnelle en grandes déformations - Application à la traction hors axes et la torsion, J. Méca. Th. et Appl., **7**, 1, 43-64, 1988.

Received January 03, 2002.

Arch. Mech., **54**, 3, pp. 245–256, Warszawa 2002

End effects in the dynamical problem of magneto-elasticity

R.QUINTANILLA

Matemática Aplicada 2 Universidad Politècnica de Catalunya,
Colón, 11. Terrassa. Barcelona. Spain
e-mail: ramon@ma2.upc.es

IN THIS PAPER we derive spatial decay bounds for the solutions of the linear dynamical problem of magneto-elasticity in a semi-infinite cylindrical region. For the forward-in-time problem we prove that an energy expression is bounded from above by a decaying exponential of a quadratic polynomial of the distance. We derive a spatial decay estimate for the backward-in-time problem as well. The proof works only if the cross-section is a finite union of rectangles with axes parallels to Ox_2 and Ox_3. As a conclusion we consider the extension of the preceding bound to the heat conduction case.

Key words: magneto-thermo-elasticity, spatial decay, comparison arguments.

1. Introduction

IN RECENT YEARS much attention has been directed to the study of end effects damping in several thermomechanical situations. The history and development of this question is explained in the work of HORGAN and KNOWLES [9] and has been periodically updated by HORGAN [7,8]. We may also recall the book of AMES and STRAUGHAN [1] where the energy method is extensively used. Here, we are interested in the coupling of elastic effects and magnetic effects. As far as the author knows, there are no contributions made to the study of spatial decay in the dynamical problem of magneto-elasticity. In this paper we derive spatial decay bounds for the solutions of the linear dynamical problem of magneto-elasticity in a semi-infinite cylindrical region. For the forward-in-time problem we prove that an energy expression is bounded above by a decaying exponential of a quadratic polynomial of the distance. We derive a spatial decay estimate for the backward in time problem as well. The proof works only if the cross-section is a finite union of rectangles with axes parallels to Ox_2 and Ox_3. The class of cylinders satisfying this condition is wide. We recall that a condition of this kind was imposed in the recent work of MUÑOZ-RIVERA and RACKE [14].

A derivation of the equations and recent papers on magneto-thermo-elasticity and isothermal magneto-elasticity can be found in [2, 4, 13, 14, 16, 22]

This paper can be considered as an extension of the method proposed in the study of several linear thermoelastic problems such as those in [17-20] and/or nonlinear viscoelasticity problems as those in [21].

This paper is of interest from the mechanical and mathematical viewpoints. Spatial estimates for the forward and backward-in-time problems of the magneto-elasticity have not been studied at present. The boundary conditions of the magnetic field (see (2.3)) put forward a new mathematical difficulty to work with. In this paper we see how to overcome it when the cross-section is a finite union of rectangles with axes parallels to Ox_2 and Ox_3.

The plan of the paper is the following: In Sec. 2 we obtain our spatial decay estimate for the forward-in-time problem. To this end we prove that a certain energy measure of the solutions satisfies a one-dimensional partial differential inequality. Comparison arguments applied to this one-dimensional partial differential equation allow us to obtain our estimate. Section 3 is devoted to the study of the backward-in-time problem. A spatial decay estimate is obtained along time-spatial lines. The extension of these arguments to the heat conduction case is sketched in the last section.

In this article we use the summation an differentiation conventions. Summation over repeated indices is assumed and the differentiation with respect to the direction x_k is denoted by $,k$. Letters in boldface stand for vectors.

2. Forward-in-time problem

We consider an initial boundary value problem for the linear magneto-elasticity. The linear partial differential equations that govern the magneto-elasticity in the case of isotropic and homogeneous material are (see [5]):

$$\rho \mathbf{u}_{,tt} - \mu \triangle \mathbf{u} - (\lambda + \mu) \nabla \mathrm{div} \mathbf{u} - \alpha [\nabla \times \mathbf{h}] \times \mathbf{H} = \mathbf{0}, \tag{2.1}$$

$$\beta \mathbf{h}_{,t} - \triangle \mathbf{h} - \beta \nabla \times [\mathbf{v} \times \mathbf{H}] = \mathbf{0}. \tag{2.2}$$

Here $\mathbf{u}$ is the displacement, $\mathbf{v} = \mathbf{u}_t$ is the velocity and $\mathbf{h}$ the magnetic field; $\mathbf{H} = (H, 0, 0)$ is a (known) constant magnetic field and $\lambda, \mu, \rho, \alpha, \beta$ are positive constants.

We study the system (2.1)-(2.2) in the semi-infinite cylinder $R = (0, \infty) \times D$, where D is a union of finite number of rectangles parallel to the x_2 and x_3 axes (see Fig. 1).

The boundary conditions are

$$\mathbf{u} = \mathbf{0}, \mathbf{h}.\mathbf{n} = 0, \ [\nabla \times \mathbf{h}] \times \mathbf{n} = \mathbf{0}, \ \text{on } (0, \infty) \times \partial D \ t > 0. \tag{2.3}$$

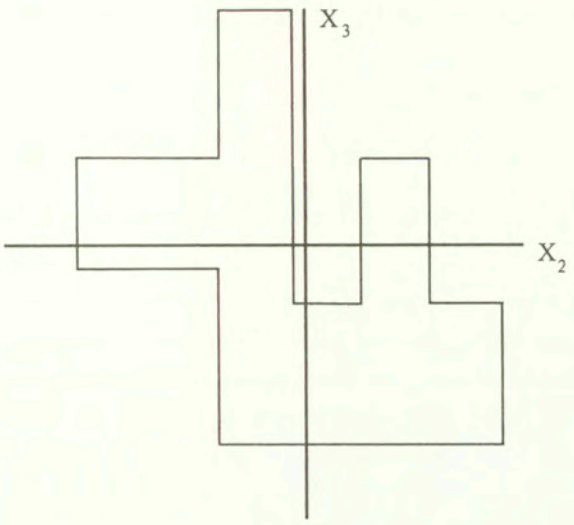

FIG. 1.

Here and from now on, let $\mathbf{n}$ be the exterior normal vector to the boundary at regular points. The initial conditions are

$$\mathbf{u}(\mathbf{x},0) = \mathbf{v}(\mathbf{x},0) = \mathbf{h}(\mathbf{x},0) = \mathbf{0} \text{ in } R. \tag{2.4}$$

Though we could impose wider asymptotic conditions, in order to make calculations easier we assume that

$$\mathbf{u}, \mathbf{v}, \mathbf{h}, \nabla\mathbf{u}, \nabla\mathbf{h} \to \mathbf{0} \text{ uniformly as } x_1 \to \infty, \text{ as } x_1^{-3}. \tag{2.5}$$

To complete the problem we should impose boundary conditions on the part of the boundary $\{0\} \times D$ for all t. But our analysis does not require the explicit knowledge of these conditions. Existence and uniqueness results for this problem could be obtained by means of semigroups methods in a similar way as in [16]. We do not consider this question here.

Now, we obtain a spatial decay estimate of the solutions of the linear problem (2.1)-(2.5). From $(2.3)_2$, we see that $h_2 n_2 + h_3 n_3 = 0$ and then $h_{2,1} n_2 + h_{3,1} n_3 = 0$. On the other hand, $(2.3)_3$ implies that

$$h_{1,2} n_2 + h_{1,3} n_3 = h_{2,1} n_2 + h_{3,1} n_3, h_{3,2} n_2 = h_{2,3} n_2, h_{3,2} n_3 = h_{2,3} n_3, \tag{2.6}$$

$$\text{on} (0,\infty) \times \partial D \; t > 0.$$

If we calculate $h_{i,2}h_i n_2 + h_{i,3}h_i n_3$ we have

$$
\begin{aligned}
(2.7)\quad & h_{i,2}h_i n_2 + h_{i,3}h_i n_3 \\
&= h_1(h_{1,2}n_2 + h_{1,3}n_3) + h_2(h_{2,2}n_2 + h_{2,3}n_3) + h_3(h_{3,2}n_2 + h_{3,3}n_3) \\
&= h_1(h_{2,1}n_2 + h_{3,1}n_3) + h_2(h_{2,2}n_2 + h_{2,3}n_3) + h_3(h_{3,2}n_2 + h_{3,3}n_3), \\
&\qquad\qquad \text{on } (0,\infty)\times\partial D,
\end{aligned}
$$

for all $t > 0$. But we know that $h_{2,1}n_2 + h_{3,1}n_3 = 0$. As we are assuming that the boundary of D consists of segments parallel to the axes, we obtain that either $n_2 = 0$ or $n_3 = 0$. If we assume (for instance) that $n_3 = 0$, then $h_2 = 0$ and $h_{2,3} = 0$ on the segment and then $h_{3,2} = 0$ on the segment. When $n_2 = 0$, we may repeat the arguments and obtain

$$
(2.8)\qquad h_{i,2}h_i n_2 + h_{i,3}h_i n_3 = 0, \quad \text{on } (0,\infty)\times\partial D,\ t > 0.
$$

It will be useful to define the matrix (σ_{ij}) by:

$$
(2.9)\qquad \sigma_{11} = \mu u_{1,1} + (\lambda+\mu)u_{j,j},\ \ \sigma_{12} = \mu u_{1,2},\ \ \sigma_{13} = \mu u_{1,3},
$$

$$
(2.10)\quad \sigma_{21} = \mu u_{2,1} + \alpha H h_2,\ \ \sigma_{22} = \mu u_{2,2} + (\lambda+\mu)u_{j,j} - \alpha H h_1,\ \ \sigma_{23} = \mu u_{2,3},
$$

$$
(2.11)\quad \sigma_{31} = \mu u_{3,1} + \alpha H h_3,\ \ \sigma_{32} = \mu u_{3,2},\ \ \sigma_{33} = \mu u_{3,3} + (\lambda+\mu)u_{j,j} - \alpha H h_1.
$$

Then equation (2.1) can be written as

$$
\sigma_{ij,j} = \rho\ddot{u}_i.
$$

We now define a function that plays a fundamental role in this section.

$$
(2.12)\qquad K(z,t) = -\int_0^t \int_{D(z)} \Big[\sigma_{i1}v_i + \frac{\alpha}{\beta}h_{i,1}h_i\Big]\,dads.
$$

Here $D(z)$ denotes the cross-section at a distance z from the origin; it has the same form as the domain D. The function $K(z,t)$ results from the vector field

$$
\Big(\sigma_{i1}v_i + \frac{\alpha}{\beta}h_{i,1}h_i, \sigma_{i2}v_i + \frac{\alpha}{\beta}h_{i,2}h_i, \sigma_{i3}v_i + \frac{\alpha}{\beta}h_{i,3}h_i\Big).
$$

Thus, in view of conditions (2.8), the divergence theorem implies that

$$K(z+h,t)-K(z,t)=-\frac{1}{2}\int\limits_{R(z+h,z)}(\rho v_i v_i+\mu u_{i,j}u_{i,j}+(\lambda+\mu)u_{i,i}u_{j,j}+\alpha h_i h_i)\,dv$$

$$-\frac{\alpha}{\beta}\int\limits_0^t\int\limits_{R(z+h,z)} h_{i,j}h_{i,j}\,dvds,$$

where

$$R(z+h,z)=\{\mathbf{x}\in R, z<x_1<z+h\}.$$

The asymptotic condition (2.5) implies that for finite time

$$\lim_{z\to\infty}K(z,t)=0. \tag{2.13}$$

Using the divergence theorem we obtain that

$$K(z,t)=\frac{1}{2}\int\limits_{R(z)}(\rho v_i v_i+\mu u_{i,j}u_{i,j}+(\lambda+\mu)u_{i,i}u_{j,j}+\alpha h_i h_i)dv \tag{2.14}$$

$$+\frac{\alpha}{\beta}\int\limits_0^t\int\limits_{R(z)} h_{i,j}h_{i,j}\,dvds.$$

Here $R(z)$ denotes the sub-region of R of the points that are at a distance greater than z from the plane $x_1=0$.

Now, we define

$$E(z,t)=\int\limits_z^\infty K(p,t)dp. \tag{2.15}$$

It follows that

$$\frac{\partial E}{\partial z}=-K(z,t), \tag{2.16}$$

and that

$$\frac{\partial^2 E}{\partial z^2}=\frac{1}{2}\int\limits_{D(z)}(\rho v_i v_i+\mu u_{i,j}u_{i,j}+(\lambda+\mu)u_{i,i}u_{j,j}+\alpha h_i h_i)da \tag{2.17}$$

$$+\frac{\alpha}{\beta}\int\limits_0^t\int\limits_{D(z)} h_{i,j}h_{i,j}\,dads.$$

From the definition of the functions K and E we also obtain that

$$\frac{\partial E}{\partial t} = -\int_{R(z)} \left[\sigma_{i1} v_i + \frac{\alpha}{\beta} h_{i,1} h_i\right] dv. \tag{2.18}$$

It is worth remarking that

$$\int_{R(z)} h_i h_{i,1} dv = -\frac{1}{2} \int_{D(z)} h_i h_i da. \tag{2.19}$$

Our next step is to estimate the time derivative of E in terms of the first two spatial derivatives of E. Using repeatedly the arithmetic-geometric mean inequality we can compute two positive constants A_1, A_2 such that

$$\begin{aligned} |\int_{R(z)} \sigma_{i1} v_i dv| &\le \frac{1}{2}\Big(\int_{R(z)} \sigma_{i1}\sigma_{i1} dv + \int_{R(z)} v_i v_i dv\Big) \\ &\le A_1(\lambda, \mu, \alpha, H, \rho) \int_{R(z)} (\rho v_i v_i + \mu u_{i,j} u_{i,j} + (\lambda + \mu) u_{i,i} u_{j,j} + \alpha h_i h_i)\, dv \\ &\le -A_1(\lambda, \mu, \alpha, H, \rho) \frac{\partial E}{\partial z}, \end{aligned} \tag{2.20}$$

and

$$\frac{1}{2} \int_{D(z)} \frac{\alpha}{\beta} h_i h_i da \le A_2(\beta) \frac{\partial^2 E}{\partial z^2}. \quad \left(A_2 = \beta^{-1}\right) \tag{2.21}$$

From (2.15)–(2.21) we obtain the inequality:

$$\frac{\partial E}{\partial t} \le -A_1 \frac{\partial E}{\partial z} + A_2 \frac{\partial^2 E}{\partial z^2}. \tag{2.22}$$

From inequality (2.22) and after the change of variable

$$w(z,t) = \exp(b_2 t - b_1 z) E(z,t), \tag{2.23}$$

where

$$b_1 = \frac{A_1}{2A_2}, \quad b_2 = b_1^2 A_2, \tag{2.24}$$

we obtain the inequality

$$\frac{\partial w}{\partial t} \le A_2 \frac{\partial^2 w}{\partial z^2}. \tag{2.25}$$

Taking into account the asymptotic behaviour of the solutions, and using comparison arguments similar to those used in the work of HORGAN *et al.* [10, 11], we obtain the estimate (see also [17, 18])

$$E(z,t) \leq \exp(b_1 z - b_2 t) \sup_{0\leq s\leq t} \Big[\exp(b_2 s) E(0,s)\Big] \frac{z}{(4\pi A_2)^{1/2}} \int_0^t (t-s)^{-3/2} \exp -\frac{z^2}{4A_2(t-s)}\, ds. \tag{2.26}$$

Some algebraic manipulations on the right-hand side of the estimate (2.26) (see [10, 11, 17, 18]), allow us to obtain the following estimate:

$$E(z,t) \leq \frac{B(t)}{z} \exp(b_1 z - \frac{z^2}{4tA_2}), \tag{2.27}$$

where

$$B(t) = (4tA_2)^{1/2} \exp(-b_2 t) \sup_{0\leq s\leq t} \Big(\exp(b_2 s) E(s,0)\Big). \tag{2.28}$$

Thus, we have proved:

THEOREM 1. *Let (u_i, h_i) be a solution of the problem determined by the system of equations (2.1), (2.2), boundary conditions (2.3) and initial conditions (2.4) such that the asymptotic condition (2.5) is satisfied. Then, the function E defined in (2.15) satisfies the estimate (2.28).*

3. Backward-in-time problem

In this section, we obtain spatial decay estimates for the backward-in-time problem. This kind of questions are relevant from a mechanical point of view when we want to have some information about what happened in the past by means of the information that we have at this moment. Thus, we study the system determined by (2.1) (which is independent of the direction of time) and the backward-in-time version of Eq. (2.2). That is

$$\beta \mathbf{h}_{,t} + \triangle \mathbf{h} - \beta \nabla \times [\mathbf{v} \times \mathbf{H}] = \mathbf{0}. \tag{3.1}$$

In this section, we deal with non-homogeneous initial conditions

$$\mathbf{u}(\mathbf{x},0) = \mathbf{u}^0(\mathbf{x}), \quad \mathbf{v}(\mathbf{x},0) = \mathbf{v}^0(\mathbf{x}), \quad \mathbf{h}(\mathbf{x},0) = \mathbf{h}^0(\mathbf{x}), \tag{3.2}$$

and the boundary conditions (2.3). We assume that

$$\int_R \Big(\rho v_i v_i + \mu u_{i,j} u_{i,j} + (\lambda+\mu) u_{i,i} u_{j,j} + \alpha h_i h_i + \frac{\alpha}{\beta} h_{i,j} h_{i,j}\Big)\, dv < \infty, \tag{3.3}$$

for all $t \geq 0$,

and that

$$\lim_{z\to\infty} \int_{D(z)} \Big(\rho v_i v_i + \mu u_{i,j} u_{i,j} + (\lambda+\mu) u_{i,i} u_{j,j} + \alpha h_i h_i + \frac{\alpha}{\beta} h_{i,j} h_{i,j}\Big)\, da = 0, \tag{3.4}$$

for all $t \geq 0$.

We consider the function

$$F_\omega(z,t) = \int_0^t \int_{R(z)} \exp(\omega s)\Big(\frac{\omega}{2}(\rho v_i v_i + \mu u_{i,j} u_{i,j} + (\lambda+\mu) u_{i,i} u_{j,j} + \alpha h_i h_i) + \frac{\alpha}{\beta} h_{i,j} h_{i,j}\Big) dv ds. \tag{3.5}$$

After a use of the divergence theorem, it follows that

$$\begin{aligned} F_\omega(z,t) = {} & \int_0^t \int_{D(z)} \exp(\omega s)(\sigma_{i1} v_i - \frac{\alpha}{\beta} h_{i,1} h_i)\, da ds \\ & - \frac{1}{2} \int_{R(z)} (\rho v_i^0 v_i^0 + \mu u_{i,j}^0 u_{i,j}^0 + (\lambda+\mu) u_{i,i}^0 u_{j,j}^0 + \alpha h_i^0 h_i^0)\, dv \\ & + \frac{1}{2} \int_{R(z)} \exp(\omega t)(\rho v_i v_i + \mu u_{i,j} u_{i,j} + (\lambda+\mu) u_{i,i} u_{j,j} + \alpha h_i h_i)\, dv. \end{aligned} \tag{3.6}$$

Several uses of the arithmetic-geometric mean inequality allow us to obtain two positive constants B_2, B_3 (that depend on $\lambda, \mu, \alpha, \beta, H, \rho, \omega$) such that

$$\int_0^t \int_{D(z)} \exp(\omega s)(\sigma_{i1} v_i - \frac{\alpha}{\beta} h_{i,1} h_i)\, da ds \leq -B_2 \frac{\partial F_\omega}{\partial z}, \tag{3.7}$$

and

$$(3.8)\quad \frac{1}{2}\int\limits_{R(z)} \exp(\omega t)(\rho v_i v_i + \mu u_{i,j}u_{i,j} + (\lambda+\mu)u_{i,i}u_{j,j} + \alpha h_i h_i)\,dv \leq B_3\frac{\partial F_\omega}{\partial t}.$$

It follows that

$$(3.9)\quad F_\omega \leq -B_2\frac{\partial F_\omega}{\partial z} + B_3\frac{\partial F_\omega}{\partial t} - S(z),$$

where

$$(3.10)\quad S(z) = \frac{1}{2}\int\limits_{R(z)} (\rho\mathbf{v}^0.\mathbf{v}^0 + \mu\nabla\mathbf{u}^0.\nabla\mathbf{u}^0 + (\lambda+\mu)(\mathrm{div}\mathbf{u}^0)^2 + \alpha\mathbf{h}^0.\mathbf{h}^0)\,dv.$$

This inequality has been studied previously (see [3, 6, 12]). Thus, we may conclude the estimate

$$(3.11)\quad F_\omega(z,t) + S(z)\Big(1 - \exp\Big(-\frac{z-z_0}{B_2}\Big)\Big) \leq F_\omega(z_0,t_0)\exp\Big(-\frac{z-z_0}{B_2}\Big),$$

that is satisfied along the line

$$(3.12)\quad z + \frac{B_2}{B_3}t = z_0 + \frac{B_2}{B_3}t_0, \quad z \geq z_0.$$

We note that (3.11) implies

$$(3.13)\quad J_\omega(z,t) + S(z)\Big(1 - \exp\Big(-\frac{z-z_0}{B_2}\Big)\Big) \leq \exp(\omega t_0)J_\omega(z_0,t_0)\exp\Big(-\frac{z-z_0}{B_2}\Big),$$

where

$$(3.14)\quad J_\omega(z,t) = \int\limits_0^t\int\limits_{R(z)} \Big(\frac{\omega}{2}(\rho v_i v_i + \mu u_{i,j}u_{i,j} + (\lambda+\mu)u_{i,i}u_{j,j} + \alpha h_i h_i) + \frac{\alpha}{\beta}h_{i,j}h_{i,j}\Big)\,dvds,$$

that is satisfied along the line (3.12).

4. Magneto-thermo-elasticity

In this section, we sketch how to extend the previous results to the case of magneto-thermo-elasticity. In this section the system of equations is:

$$\rho \mathbf{u}_{,tt} - \mu \triangle \mathbf{u} - (\lambda + \mu) \nabla \mathrm{div} \mathbf{u} - \alpha [\nabla \times \mathbf{h}] \times \mathbf{H} + \gamma \nabla \theta = \mathbf{0}, \tag{4.1}$$

$$\theta_{,t} - k \triangle \theta + \gamma \mathrm{div} \mathbf{v} = 0, \tag{4.2}$$

and Eq. (2.2) as well. Here θ is the temperature measured with respect to a uniform reference temperature in the reference configuration, and γ is an arbitrary real number.

For the forward-in-time problem we supplement the boundary and the initial conditions (2.3), (2.4) with homogeneous boundary and initial conditions on the temperature

$$\theta(\mathbf{x}, 0) = 0, \quad \mathbf{x} \in R \quad \text{and} \quad \theta(\mathbf{x}, t) = 0, \quad \mathbf{x} \in (0, \infty) \times \partial D, \tag{4.3}$$

and supplement the asymptotic condition (2.5) with

$$\theta, \nabla \theta \to \mathbf{0} \text{ uniformly as } x_1 \to \infty \text{ as } x_1^{-3}. \tag{4.4}$$

If we define

$$K_\theta(z,t) = K(z,t) - \int_0^t \int_{D(z)} k \theta_{,1} \theta \, da ds. \tag{4.5}$$

It follows that

$$K_\theta(z,t) = \frac{1}{2} \int_{R(z)} (\rho v_i v_i + \mu u_{i,j} u_{i,j} + (\lambda + \mu) u_{i,i} u_{j,j} + \theta^2 + \alpha h_i h_i) \, dv + \int_0^t \int_{R(z)} \left(k \theta^2 + \frac{\alpha}{\beta} h_{i,j} h_{i,j} \right) dv ds. \tag{4.6}$$

If we define

$$E_\theta(z,t) = \int_z^\infty K_\theta(p,t) \, dp, \tag{4.7}$$

we may obtain an inequality of type (2.22), but now the parameters A_1 and A_2 (and consequently b_1 and b_2) may also depend on k and γ. Estimates of type (2.26), (2.28) can also be obtained in this case.

For the backward-in-time problem we assume the initial conditions (3.2) and we can supplement them by non-homogeneous initial conditions on the temperature θ. The analysis starts by assuming conditions similar to (3.3) and (3.4) and considering the function

$$(4.8)\quad G_\omega(z,t) = \int_0^t \int_{R(z)} \exp(\omega s)\Big(\frac{\omega}{2}\big(\rho v_i v_i + \mu u_{i,j}u_{i,j} + (\lambda+\mu)u_{i,i}u_{j,j} + \alpha h_i h_i + \theta^2\big) + \frac{\alpha}{\beta}h_{i,j}h_{i,j} + k\theta_{,i}\theta_{,i}\Big)\,dvds.$$

Two estimates similar to (3.11) and (3.13) can be obtained. The parameters B_2, B_3 also depend on the new constitutive constants γ and k.

Acknowledgements

This work is supported by the project "Aspectos Matemáticos en las teorías termomecánicas generalizadas" (BFM2000-0809).

References

1. K. A. AMES and B. STRAUGHAN, *Non-standard and improperly posed problems*, Academic Press, San Diego 1997.
2. E. ANDREOU and G. DASSIOS, *Dissipation of energy for magnetoelastic waves in a conductive medium*, Quart. Appl. Math., **55**, 23-39, 1997.
3. F. BOFILL and R. QUINTANILLA, *On a backward in time problem arising in viscoelasticity*, Mathematics and numerical aspects of wave propagation, A.BERMÚDEZ, D. GÓMEZ, C. HAZARD, P. JOLY and J. E. ROBERTS, [Eds.] SIAM 123-127, 2000.
4. S. CHANDLER, *Phase velocity and energy loss in magneto-thermo-elastic waves*, Int. Jour. Eng, Sci., **6**, 409-424, 1968.
5. C. A. ERINGEN and G. A. MAUGIN, *Electrodynamics of continua I*, Springer-Verlag, New-York 1990.
6. F. FRANCHI AND B. STRAUGHAN, *Spatial decay estimates and continuous dependence for an equation from dynamo theory*, Proc. Royal Society London A, **445**, 437-451, 1984.
7. C. O. HORGAN, *Recent developments concerning Saint-Venant's Principle: An update*, Applied Mechanics Reviews, **42**, 295-303, 1989.
8. C.O. HORGAN, *Recent developments concerning Saint-Venant's Principle: A second update*, Applied Mechanics Reviews, **49**, 101-111, 1996.

9. C. O. HORGAN and J. K. KNOWLES, *Recent developments concerning Saint-Venant's Principle*, Advances in Applied Mechanics, J. W. HUTCHINSON and T. Y. WU, [Eds.] 23 Academic Press pp. 179-269, New York 1983.

10. C. O. HORGAN, L. E. PAYNE and L. T. WHEELER, *Spatial decay estimates in transient heat conduction*, Quart. Appl. Math., **42**, 119-127, 1984.

11. C. O. HORGAN and R. QUINTANILLA, *Spatial decay of transient end effects in functionally graded heat conducting materials*, Quat. Appl. Math., **XIL**, 529-542, 2001.

12. C. LIN and L. PAYNE, *On the spatial decay of ill-posed parabolic problems*, Math. Models and Methods in Applied Science, **3**, 563-575, 1993.

13. J. E. MUÑOZ RIVERA and R. RACKE, *Magento-thermo-elasticity; Large-time behavior for linear systems*, Advances in Differential Equations, **6**, 359-384, 2001.

14. J. E. MUÑOZ RIVERA and R. RACKE, *Polynomial stability in two-dimensional magneto-elasticity*, Universitat Konstanz, **117**, 2000.

15. G. PARIA, *Magneto-elasticity and magneto-thermo-elasticity*, Advances in Appl. Mechanics, **10**, 73-112, 1967.

16. G. PERLA MENZALA and E. ZUAZUA, *Energy decay of magnetoelastic waves in a bounded conductive medium*, Asymptotic Analysis, **18**, 349-362, 1998.

17. R. QUINTANILLA, *End effects in thermoelasticity*, Mathematical Methods in Applied Sciences, **24**, 93-102, 2001.

18. R. QUINTANILLA, *Damping of end effects in a thermoelastic theory*, Applied Mathematics Letters, **14**, 137-141, 2001.

19. R. QUINTANILLA, *On the spatial decay for the dynamical problem of thermo-microstretch elastic solids*, Int. J. Engng. Sci., **40**, 109-121, 2002.

20. R. QUINTANILLA, *Spatial asymptotic behaviour in incremental thermoelasticity*, Asympt. Anal., **27**, 265-279, 2001.

21. R. QUINTANILLA, *Comparison arguments in nonlinear viscoelasticity*, Manuscript 2001.

22. A. J. WILSON, *The propagation of magneto-thermo-elastic plane waves*, Proc. Camb. Phil. Soc., **59**, 483-488, 1963.

Received August 3, 2001; revised version April 19, 2002.

Thermal Stresses 2003

CALL FOR PAPERS

Fifth International Congress on Thermal Stresses and Related Topics
http://www.esm.vt.edu/ts2003/

Blacksburg, Virginia, USA
June 8 - 11, 2003
hosted by the Department of Engineering Science and Mechanics
Virginia Polytechnic Institute and State University

Abstracts: Participants who wish to contribute a paper are requested to submit an abstract (about 500 words with 4 or 5 key words) including figures, tables and references, by mail, telefax, or E-mail to: ts2003@vt.edu. When the abstract is submitted by mail, two copies are required. The abstracts should be mailed to:

Mrs. Lisa Smith, TS2003, Virginia Tech, 219 ESM Department, Blacksburg, VA 24061, E-mail: ts2003@vt.edu

The abstract should include the title, full name of the author(s), affiliation, mailing address, telephone and telefax numbers, and E-mail address. See the web page of the Congress for the abstract format.

Deadlines:

Final date for receipt of abstracts: September 30, 2002 Authors informed concerning acceptance: November 15, 2002 Final date for receipt of camera-ready manuscript: January 31, 2003

Inquires regarding the program should be directed to:

Professor Liviu Librescu, General Chair of the Congress, Engineering Science and Mechanics, VIRGINIA POLYTECHNIC INSTITUTE AND STATE UNIVERSITY, Blacksburg, VA. 24061-0219, USA
Phone: (540) 231-5916, Telefax: (540) 231-4574, E-mail: librescu@vt.edu

IUTAM

International Congress of Theoretical and Applied Mechanics

August 15 - 21, 2004 ♦ Warsaw, Poland

President:	*Co-Chairman:*	*Co-Chairman:*	*Secretary-General:*
Witold Gutkowski	Michał Kleiber	Włodzimierz Kurnik	Tomasz Kowalewski
PAN, Warszawa	*IPPT PAN, Warszawa*	*Politechnika Warszawska*	*IPPT PAN, Warszawa*

Preliminary Announcement

Scientific Program

The scientific program will start and end with opening and closing lectures, presented by prominent scientists. Titles of lectures and names of lecturers will be announced in October 2002, in the First Announcement and Call for Papers for the Congress.

The program will consist, moreover, of sectional lectures, mini-symposia and contributed papers presented in lecture and seminar presentation sessions. Invitations to present the contributed papers will be made on the recommendation of the International Paper Committee, based on their reviews of submitted abstracts and extended summaries.

Mini-Symposia

- Smart materials and structures.
- Tissue, cellular and molecular biomechanics.
- Mechanics of thin films and nanostructures.
- Microfluidics.
- Microgravity flow phenomena.
- Atmosphere and ocean dynamics.

Pre-Nominated Sessions

In Fluid Mechanics

Biological fluid dynamics • Boundary layers • Combustion and flames • Complex and smart fluids • Compressible flow • Computational fluid dynamics (jointly with IACM) • Convective phenomena • Drops and bubbles • Environmental fluid mechanics • Experimental methods in fluid mechanics • Flow control • Flow in porous media • Flow instability and transition • Flow in thin films • Fluid mechanics of materials processing • Granular flows • Low-Reynolds-number flow • Magnetohydrodynamics • Multiphase flows • Solidification and crystalgrowth • Stirring and mixing • Suspension mechanics • Topological fluid mechanics • Turbulence • Vortex dynamics • Waves

In Solid Mechanics

Computational solid mechanics (jointly with IACM) • Contact and friction problems (jointly with IAVSD)g • Control of multibody systems • Control of structures • Damage mechanics • Dynamic plasticity of structures • Elasticity • Experimental methods in solid mechanics • Fatigue • Fracture and crack mechanics (jointly with ICF) • Functionally graded materials • Impact and wave propagation • Material instabilities • Mechanics of composites • Mechanics of phase transformations (jointly with IACM) • Mechanics of porous materials • Multibody dynamics • Plasticity and viscoplasticity • Plates and shells (jointly with IACM) • Rock mechanics and geomechanics • Solid mechanics in manufacturing • Stability of structures • Stochastic micromechanics • Structural optimization (jointly with ISSMO) • Structural vibrations • Viscoelasticity and creep

Topics involving both fluid mechanics and solid mechanics

Acoustics • Chaos in fluid and solid mechanics • Continuum mechanics • Fluid-structure interaction • Mechanics of foams and cellular materials • Multiscale phenomena in mechanics

Details on preparation of manuscripts will be provided in the First Announcement and Call for Papers in October 2002.

It is planned to provide all future information mostly by e-mail. If you are interested in receiving future information, ***please pre-register on the Congress World Wide Web site*****:**

http://ictam04.ippt.gov.pl

On this site, you can already find many interesting information concerning the Congress

Correspondence related to the Congress should be sent to:

Prof. Tomasz Kowalewski, ICTAM04 Secretary-General
Institute of Fundamental Technological Research
Świętokrzyska 21, 00-049 Warszawa, Poland
e-mail: ictam04@ippt.gov.pl

Received August 3, 2001; revised version April 19, 2002.

INSTITUTE OF FUNDAMENTAL TECHNOLOGICAL RESEARCH
publishes the following periodicals:

ARCHIVES OF MECHANICS — bimonthly (in English)
ARCHIVES OF ACOUSTICS — quarterly (in English)
ARCHIVES OF CIVIL ENGINEERING — quarterly (in English)
ENGINEERING TRANSACTIONS — quarterly (in English)
COMPUTER ASSISTED MECHANICS AND ENGINEERING SCIENCES — quarterly (in English)
JOURNAL OF TECHNICAL PHYSICS — quarterly (in English)

Subscription orders for all journals edited by IFTR may be sent directly to:
Editorial Office
Institute of Fundamental Technological Research
Świętokrzyska 21, p. 508
00-049 Warszawa, POLAND

DIRECTIONS FOR THE AUTHORS

The journal *ARCHIVES OF MECHANICS* (ARCHIWUM MECHANIKI STOSOWANEJ) deals with the printing of original papers which should not appear in other periodicals.

As a rule, the volume of a paper should not exceed 40 000 typographic signs, that is about 20 type-written pages, format: 210×297 mm, leaded. The papers should be submitted in two copies. They must be set in accordance with the norms established by the Editorial Office. Special importance is attached to the following directions:

1. The title of the paper should be as short as possible.
2. The text should be preceded by a brief introduction; it is also desirable that a list of notations used in the paper should be given.
3. The formula number consists of two figures: the first represents the section number and the other the formula number in that section. Thus the division into subsections does not influence the numbering of formulae. Only such formulae should be numbered to which the author refers throughout the paper, and also the resulting formulae. The formula number should be written on the left-hand side of the formula; round brackets are necessary to avoid any misunderstanding. For instance, if the author refers to the third formula of the set (2.1), a subscript should be added to denote the formula, viz. $(2.1)_3$.
4. All the notations should be written very distinctly. Special care must be taken to write small and capital letters as precisely as possible. Semi-bold type should be underlined in black pencil. Explanations should be given on the margin of the manuscript in case of special type face.
5. It has been established to denote vectors by semi-bold type. Trigonometric functions are denoted by sin, cos, tg and ctg, inverse functions – by arc sin, arc cos, arc tg and arc ctg; hyperbolic functions are denoted by sh, ch, th and cth, inverse functions – by Arsh, Arch, Arth and Arcth.
6. Figures in square brackets denote reference titles. Items appearing in the reference list should include the initials of the first name of the author and his surname, also the full title of the paper (in the language of the original paper); moreover;
   a) In the case of books, the publisher's name, the place and year of publication should be given, e.g., 5. S. ZIEMBA, *Vibration analysis*, PWN, Warszawa 1970;
   b) In the case of a periodical, the full title of the periodical, consecutive volume number, current issue number, pp. from ... to ..., year of publication should be mentioned; the annual volume number must be marked in black pencil so as to distinguish it from the current issue number, e.g., 6. M. SOKOŁOWSKI, *A thermoelastic problem for a strip with discontinuous boundary conditions*, Arch. Mech., **13**, 3, 337–354, 1961.
7. The authors should enclose a summary of the paper. The volume of the summary is to be about 100 words.
8. The authors are kindly requested to enclose the figures prepared on diskettes (format WMF, EMF, GIF, PCX, BitMaP, EPS or PostScript).

Upon receipt of the paper, the Editorial Office forwards it to the reviewer. His opinion is the basis for the Editorial Committee to determine whether the paper can be accepted for publication or not.

The printing of the paper completed, the author receives 25 copies of reprints free of charge. The authors wishing to get more copies should advise the Editorial Office accordingly, not later than the date of obtaining the galley proofs.

The papers submitted for publication in the journal should be written in English. No royalty is paid to the authors. Please send us, in addition to the typescript, the same text prepared on a diskette (floppy disk) 3 1/2" as an ASCII file, preferably in the TEXor LATEXformat in Dos or Unix format.

EDITORIAL COMMITTEE
ARCHIVES OF MECHANICS
(ARCHIWUM MECHANIKI STOSOWANEJ)

Archives of Mechanics

Contents of issue 3 vol. 54

185 RAJNEESH KUMAR and SUMAN CHOUDHARY, *Influence and Green's functions for orthotropic micropolar continua*

199 J. SZUMBARSKI, *Immersed boundary approach to stability equations for a spatially periodic viscous flow*

223 A. CHENAOUI, F. SIDOROFF, M. DARRIEULAT, A. HIHI, *The plane single crystal under off-axis uniaxial tension*

245 R.QUINTANILLA, *End effects in the dynamical problem of magneto-elasticity*

Arch. Mech., **54**, nr 3, str. 183–263, Warszawa 2002